UNIVERSITÀ DEGLI STUDI DI PADOVA

Department of Industrial Engineering DII

Master degree in Mechanical Engineering

A double-source heat pump prototype coupled to PVT collectors using R744 as the refrigerant

Supervisor: Prof. Angelo Zarrella

Co-supervisor: Eng. Sara Bordignon

Laureando: Alberto Bisi

Matricola : 2027542

Academic Year 2022/2023

Abstract

Reducing greenhouse gas emissions and the energy consumption is crucial in mitigating the effects of climate change and global warming. Multi-source systems coupled with heat pumps that use natural refrigerants offer an attractive solution for the residential sector.

In this work, a model of a multi-source plant was developed using TRNSYS. The considered heat pump is a dual-source unit capable of working with an air-finned coil heat exchanger or, alternatively, with photovoltaic-thermal (PVT) solar collectors as the evaporator. The refrigerant is directly evaporated in three PVT panels exploiting solar energy. These panels consist of a sheet-and-tube heat exchanger made of an aluminum plate and a copper serpentine located beneath the PV module. This setup enables the utilization of solar radiation to evaporate the refrigerant and enhance the electricity production of the PV cells by cooling them.

The PVT panel and CO2 heat pump models were incorporated into a novel TRNSYS component. The heat pump prototype's operation is analyzed through steady and dynamic simulations. The model of the heat pump coupled to the finned coil and PVT panels are calibrated and validated against measurements.

Dynamic simulations are performed considering the heat pump's long-term operation, using Venice's test reference year weather data.

Nomenclature

Symbols

A	area [m^2]	KA	heat transfer coefficient/exchange area product [W·K^{-1}]
a_x	finned coil evaporator efficiency empirical coefficients	l	serpentine length [m]
b_{pv}	temperature coeffic	$\dot{m}$	mass flow rate [kg·s^{-1}]
c_p	specific heat capacity [J·kg^{-1}·K^{-1}]	n	number of discretized elements/node
C_x	compressor polynomials empirical coefficients	N	number of plates [-]
D	internal diameter [m]	P	electrical power [W]
G	incident solar radiation [W·m^{-2}]	p	pressure [bar]
GA	absorbed solar radiation [W]	Q	heat flow rate [W]
h	specific enthalpy [J·kg^{-1}]	R	thermal resistance [m^2·K·W^{-1}]
H	global transmission coefficient [W·m^{-2}·K^{-1}]	T	temperature [°C]
htc	local heat transfer coefficient [W·m^{-2}·K^{-1}]	t	thickness [m]
K	global heat transfer coefficient [W·m^{-2}·K^{-1}]	v	wind velocity [m s^{-1}]

Greek symbols

α	absorption coefficient [-]	$\overline{\tau\alpha}$	the ratio of absorbed solar radiation [-]
η	efficiency [-]	σ	Stefan-Boltzmann constant [W·m^{-2}·K^{-4}]
λ	thermal conductivity [W·m^{-1}·K^{-1}]	β	slope angle [°]
ρ	density [kg·m^{-3}], reflection coefficient [-]	τ	transmission coefficient [-]

Subscripts/Superscripts

air	air	sky	equivalent sky
c	compressor	r	refrigerant
e	evaporation	s	simulated value
fin	equivalent fin	suc	compressor suction
gc	gas-cooler	abs	absorber plate
g	glass	T1	TANK1
guess	tentative	T2	TANK2
HE	user heat exchanger	tot	total
i	plate discretized element/iteration	user	user load
in	inlet	w	water
dis	compressor discharge	EVA	ethylene vinyl acetate
int	internal heat exchanger	ref	reference

lam	throttling valve	pipe	refrigerant pipe
m	measured value	we	welding
max	maximum	start	starting value
out	outlet	node	PVT node
p	plate		

Acronyms /Abbreviations

PV	photovoltaic	USER	user heat exchanger
PVT	photovoltaic-thermal collector	TANK	water tank
COMP	compressor	DX-SAHP	direct-expansion solar-assisted heat pump
COP	coefficient of performance	GWP	global warming potential
GC	gas-cooler	HFC	hydrofluorocarbons
INT	internal heat exchanger	ODP	ozone-depleting potential
EEV	electronic expansion valve	LCA	life cycle assessment
REC	low-pressure receiver tank	MPPT	maximum power point tracking
RMSE	root mean square error		

Index

1 Introduction 1
  1.1 Heat pump 5
  1.2 Refrigerant choice 6
    1.2.1 Refrigerant history 6
    1.2.2 CO_2 as refrigerant 7
  1.3 Multisource heat pump 8
    1.3.1 Photovoltaic-thermal (PVT) 9
  1.4 Multisource heat pump and PVT 11
2 Heat pump prototype 15
  2.1 Cycle explanation 15
  2.2.Heat exchanger 18
  2.3.Data collection 19
3 Numerical model 23
  3.1 Heat pump model 23
  3.2 PVT model 25
    3.2.1 The energy balance on the glass node 26
    3.2.2 The energy balance of the PV node 27
    3.2.3 The energy balance of the absorber plate node 28
    3.2.4 The energy balance of the fluid node 28
5 Heat pump - TRNSYS model 31
  5.1 Experimental test 35
    5.1.1 Finned coil test 35
    5.1.2 PVT test 37
  5.2 Model validation 39
    5.2.1 PVT validation 39
    5.2.3 Finned coil simulation 46
    5.2.4 PVT simulation 47
6. Seasonal simulation 51
  6.1 Results of seasonal simulation 56
7. Conclusion 65

1 Introduction

Climate change is happening faster than expected leading to increasingly noticeable impacts, such as the severe drought and temperature rise currently afflicting Italy. Mitigating these effects requires a reduction in greenhouse gas emissions and energy consumption, which remains the primary solution. To achieve a more sustainable future, every country must implement new laws and guidelines to promote sustainable practices.

The first step was made with the Kyoto protocol, adopted in 1997 and entered into force in 2005, whose main objective was to reduce the onset of global warming by reducing greenhouse gas concentrations in the atmosphere [1]. On 12 December 2015, 196 Parties at the UN Climate Change Conference (COP21) in Paris, France, agreed to the Paris agreement, whose main objective is to hold "the increase in the global average temperature to well below 2°C above pre-industrial levels" and to reduce greenhouse gas emissions by at least 40% by 2030 compared to the pre-industrial period. However, in recent years, world leaders have stressed the need to limit global warming to 1,5°C by the end of the century. To achieve this goal, greenhouse emissions must peak before 2025 [2]. Only strong actions will lead to achieve this goal, and each country has to work lowering their greenhouse gas emissions and energy consumption, favouring renewable resources and providing new climate policy.

The introduction of the Renewable Energy Directive (2009/28/EC) in 2009, push the deployment of renewables ending In a yearly growth, reaching more than 22% in 2020. The 2022 study 'EU's global leadership in renewables' confirms that the EU is in a leading position for renewables technology development and deployment, but suggests that its competitive position on global renewable energy markets could be further strengthened.

The Renewable Energy Directive was revised in 2018 and take effect since June 2021.The existing directive sets the overarching European target for renewable energy and includes rules to ensure the uptake of renewables in the transport sector and in heating and cooling, as well as common principles and rules for renewables support schemes, the rights to produce and consume renewable energy and to establish renewable energy communities, and sustainability criteria for biomass. The directive also establishes rules to remove barriers, stimulate investments and drive cost reductions in renewable energy technologies

In July 2021, the Commission proposed another revision to accelerate the take-up of renewables in the EU and to help reaching the 2030 energy and climate objectives. The directive sets a common target for the amount of renewable energy in the EU's energy consumption by 2030 (32%). In May 2022 the Commission proposed in its Communication on the REPowerEU plans to increase again this target to 45% by 2030. This directive provides the guidelines to achieve the EU's objective of climate neutrality by 2050.[3]
It's important to remember that In 2015 the United Nation General Assembly adopted the Sustainable Development Goals (SDGs), an action plan for international cooperation used to achieve a sustainable future for our planet. It is made of 17 SDGs and one SDGs it's about Energy: the global goal on energy - SDG 7 – has three main targets: ensure affordable, reliable and universal access to modern energy services; increase the share of renewable energy in the global energy mix; improve the energy efficiency.[4]

An instrument that can be employed to verify climate change progress in different countries is the Climate Change Performance index (CCPI), which promotes transparency in national and international climate politics [5]. The CCPI provides standardized guidelines to compare the climate performance of 59 countries and the EU, which are responsible for 92% of global greenhouse gas emissions. Through the use of standardized criteria, the CCPI assesses four categories, consisting of 14 indicators: Greenhouse Gas Emissions (40% of the overall score), Renewable Energy (20%), Energy Use (20%), and Climate Policy (20%). Unfortunately, no country currently meets the requirements of the Paris Agreement, which is to limit global warming to well below 2 °C, this is why the first three places in the final ranking remain unoccupied. In 2023 Italy rises one spot to 29th in the CCPI rank, first place for Denmark, but its reliance on fossil gas as a bridge fuel, the lack of a clear climate policy to reduce greenhouse gasses emissions and raise the share of renewable energy attracted criticism from climate experts.

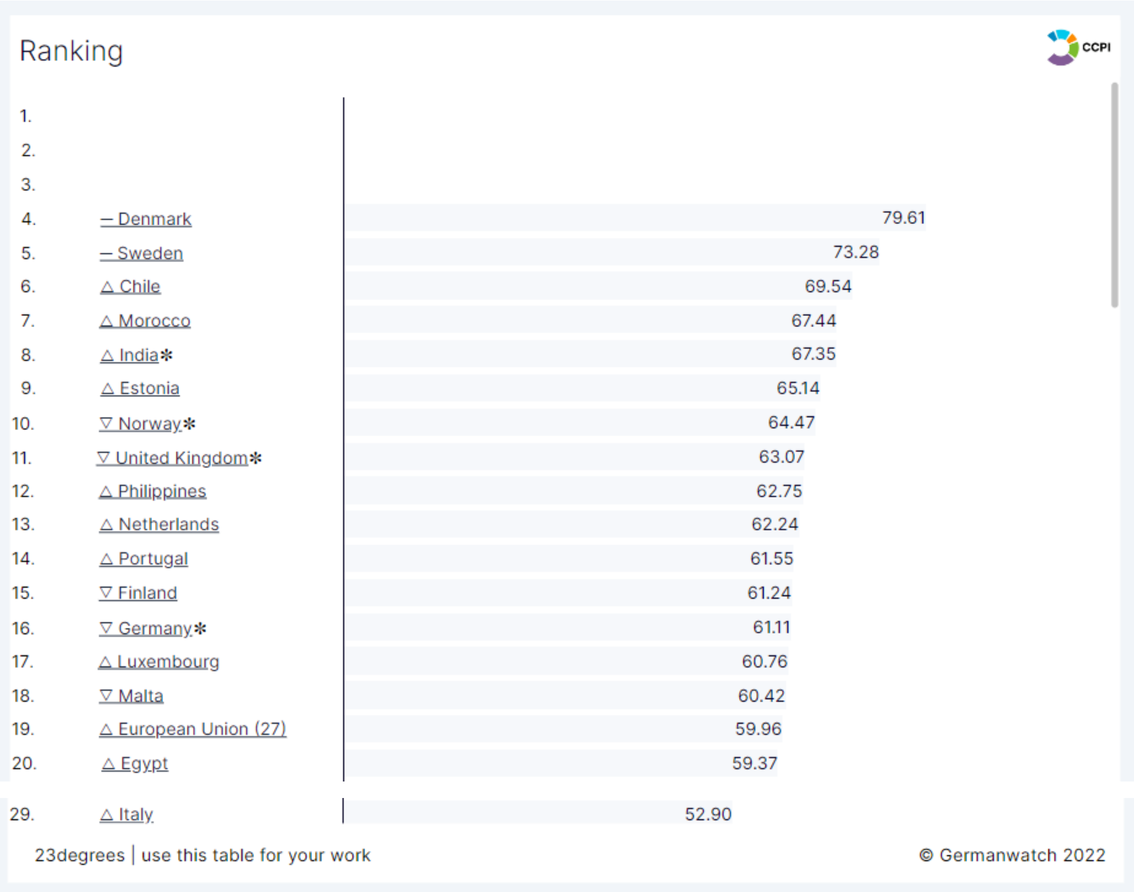

Ranking

1.		
2.		
3.		
4.	– Denmark	79.61
5.	– Sweden	73.28
6.	△ Chile	69.54
7.	△ Morocco	67.44
8.	△ India✻	67.35
9.	△ Estonia	65.14
10.	▽ Norway✻	64.47
11.	▽ United Kingdom✻	63.07
12.	△ Philippines	62.75
13.	△ Netherlands	62.24
14.	△ Portugal	61.55
15.	▽ Finland	61.24
16.	▽ Germany✻	61.11
17.	△ Luxembourg	60.76
18.	▽ Malta	60.42
19.	△ European Union (27)	59.96
20.	△ Egypt	59.37
29.	△ Italy	52.90

23degrees | use this table for your work

© Germanwatch 2022

FIGURE(1) : CCPI ranking [5]

Nowadays a lot of effort is being made to improve our heating and cooling systems: heating and cooling, in Europe, generate nearly half of the total energy consumption and much of it is wasted: in 2012 546 Mtoe of final energy consumption, equal to the 50%, came from this sector and remained so in recent years[6].

In 2021 half of energy demand for buildings was used for space and water heating, leading to 2 450 Mt of direct CO2 emissions. This results from the over 60% of heating energy demand covered by fossil fuels [7]Developing a strategy to make heating and cooling more efficient/sustainable have become more and more important indeed this sector is rapidly moving to clean low carbon energy.   In 2020 the 23% of the total energy used for heating and cooling in the EU and the 20% in Italy came from renewable resources. In 2021 the gross consumption of all fuels increased mainly due to economic recovery after lifting COVID-19 restrictions and the share of renewable decreased to 22.9%. The value of 2004 (11.7%) has almost doubled.

It’s particularly encouraging to see that Sweden, Estonia, Latvia, and Finland have made significant progress in using renewable energy for heating and cooling. This shows that it’s possible for countries to make significant progress towards using renewable energy in heating and cooling by adopting appropriate technologies and policies. For sure the developments in the industrial sector, services and households (including the electrification of heating by using heat pumps) contributed to the growth of this process [8], [9]

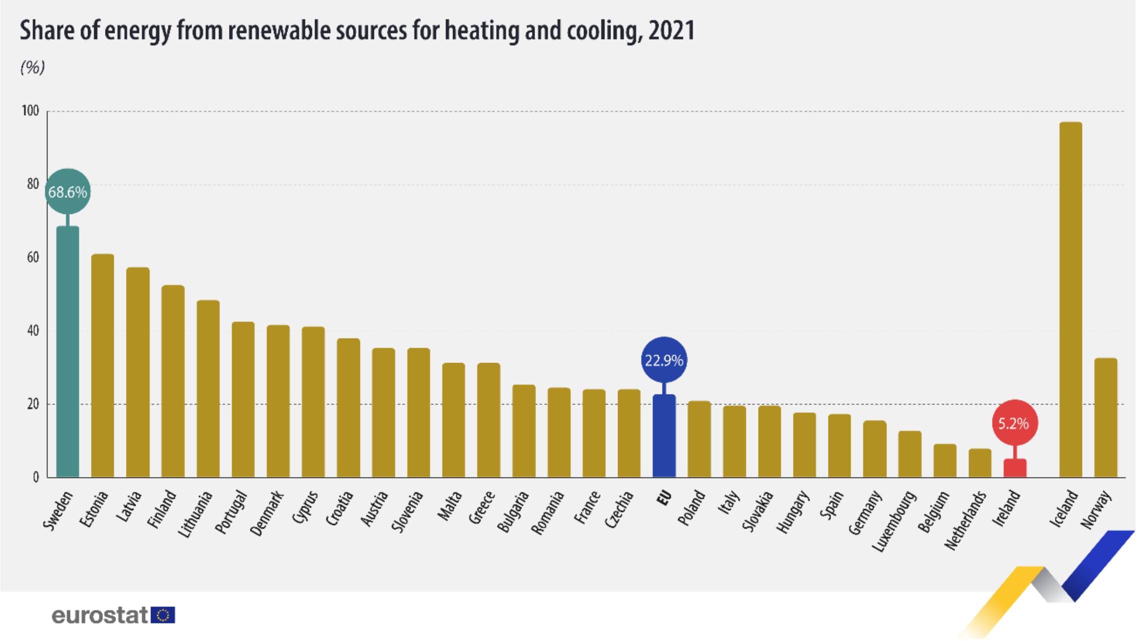

FIGURE(2) : Share of renewable sources for heating and cooling, 2021 [9]

Heat pumps, powered by low-emissions electricity, are the central technology in the global transition to secure a sustainable heating. In 2021 around 10% of space heating need were covered by this technology.

1.1 Heat pump

A heat pump is a device that can provide heating, cooling and hot water for residential, commercial and industrial use. All heat pump can provide heating and cooling, let's consider the heating operation. The operating cycle is known as the "refrigerant cycle" which has four phase: evaporation, compression, condensation, expansion. In the evaporator the refrigerant evaporates extracting heat from the heat sink, then the refrigerant is sent to the compressor where the refrigerant gas is compressed to a high pressure, which leads to a rise in temperature. On the discharge side of the compressor, vapour which is now hot and highly pressurised passes through the second heat exchanger, called the condenser. Here the refrigerant release the heat to a heat sink, this heat will be used by the heating system of the house. Finally the condensed refrigerant passes through an expansion valve, turning back to liquid phase, and so the cycle begin again[10], [11].

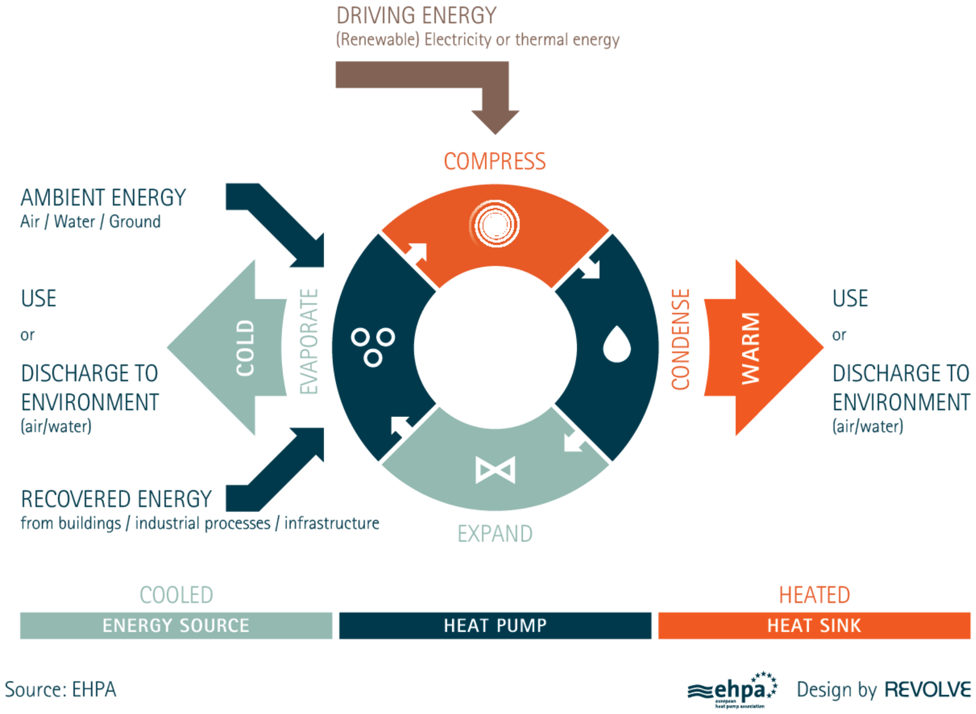
DRIVING ENERGY
(Renewable) Electricity or thermal energy
COMPRESS
AMBIENT ENERGY
Air / Water / Ground
USE
or
DISCHARGE TO
ENVIRONMENT
(air/water)
COLD
EVAPORATE
CONDENSE
WARM
USE
or
DISCHARGE TO
ENVIRONMENT
(air/water)
RECOVERED ENERGY
from buildings / industrial processes / infrastructure
EXPAND
COOLED
ENERGY SOURCE
HEAT PUMP
HEATED
HEAT SINK
Source: EHPA
ehpa
Design by REVOLVE

FIGURE(3) : How a heat pump works [11]

In Figure(3) a simplified scheme of heat pump is shown, in heating mode the useful effect is at the condenser where heat is rejected usually to water/air in order to heat up the room. There are many different heat sources that can be used, the most common is air followed by geothermal energy and energy stored in a river or a lake. It is possible also to recover wasted heat from industrial process, industrial process and buildings. Because most of the heat is transferred rather than generated, heat pumps are far more efficient than conventional heating technologies such as boilers or electric heaters and can be cheaper to run. The energy output, heat, is normally greater than the required power, mainly electricity used to run the compressor resulting in a high value of the coefficient of performance (COP). If the electricity used comes from renewable resources, as an example solar or wind energy, then the heat pump uses 100% renewables and is carbon neutral [11].

1.2 Refrigerant choice

The working fluid in the "refrigerant cycle" has to satisfy a number of requirement that can be divided into two groups [12]:

- The refrigerant shouldn't cause any risk of injuries, fire or property damages in case of leakage
- The chemical, physical and thermodynamical properties of the refrigerant have to be suitable for the system at the working conditions.

1.2.1 Refrigerant history

Until 1922 the working fluid in vapor compression cycles was only ammonia (NH_3), carbon dioxide (CO_2), sulphur dioxide (SO_2) and water. Around 1922 methyl chloride (CH_3CL) and ethyl chloride (C_2H_5Cl) were introduced, they can be seen as chlorofluorocarbons (CFCs) precursors. In 1928 Thomas Midgley, a research engineer with a subsidiary of General Motors, defined that just eight elements were possible to use to produce refrigerants: carbon, nitrogen, oxygen, sulphur, hydrogens, fluorine, chlorine and bromine. In 1930 at the meeting of the American Chemical society Midgley presented a new refrigerant R12. This was the beginning of the massive use of CFCs and HCFCs (as R22) in modern refrigeration cycles. In December 1973 F. Sherwood Rowland and Mario Molina presented a theory claiming that CFCs would deplete the ozone layer, this theory will led them to win a Nobel prize. The Montreal protocol in 1987 and later the London and Copenhagen Amendment in 1900 and 1992 led to banning CFCs and reduce the share HCFCs used. From this moment new Chlorine-free substances were developed, R12 is now replaced with R134a. Replacing R22 is more difficult, one possibility is to use propane (R290) but this natural gas is flammable. [12]

The depletion of the stratospheric ozone layer and global warming have both increased the interest on natural refrigerants , such as the "old" ammonia and carbon dioxide. Recent regulations such as the Regulation No 517 of the European Union of 2014, as well as the Kigali Amendment of the United Nations of 2016 are promoting the adoption of refrigerants with low global warming potential and the gradual reduction of hydrofluorocarbons (HFCs)[13] .

1.2.2 CO_2 as refrigerant

Carbon dioxide gives a good compromise in terms of characteristics as working fluid [12]:

- CO_2 is compatible with common material used in the refrigerant circuit and allows to use traditional lubricants.
- CO_2, also called R744 when speaking about refrigerant, is abundant, easily available and cheap. It is a natural compound not harmful toward biosphere. It has an Ozone Depleting Potential, ODP=0 and a Global Warming Potential, GWP=1. CO_2 is the reference compounds for the calculation of the GWP, this explains why its value is 1.

  ASHRAE [14]assigns numbers and safety classification to the refrigerants based on toxicity (A=lower toxicity, B=higher toxicity) and flammability (1=no flame propagation, 2=lower flammability, 3=higher flammability):

  Carbon dioxide is classified as A1: low flammability and low toxicity.

Here a comparison with other used refrigerants used in heat pumps [15]

REFRIGERANT	ASHRAE SAFETY GROUP	GWP	ODP
R744	A1	1	0
R290	A3	3	0
R134a	A1	1430	0
R32	A2	675	0
R22	A1	1800	0.05

Table(1) : Refrigerant characteristics [15]

CO_2 has a low critical temperature (31,06°C) and a high working pressure, which can be as high as 120 bar in standard applications. For this reason in requires a careful attention in the design of the system components.

Because of its low critical temperature the ideal vapor compression cycle doesn’t perform well. A transcritical cycle is preferred [16] .

.

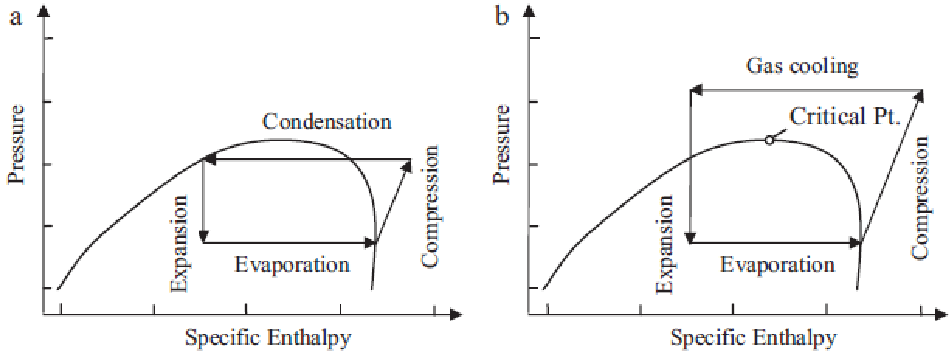

FIGURE(4) : P-h diagrams showing: (a) subcritical cycle ; (b) transcritical cycle [16]

In Figure(4) is presented the main difference between a traditional subcritical cycle (a) and a transcritical cycle (b): as shown in (b) no condensation occurs, instead of a condenser there is a gas cooler, in this heat exchanger the vapor CO_2 is cooled down without changing its phase. Based on their numerical analysis, Liu et al. [17] discovered that while the COP of a fundamental CO2 transcritical cycle is inferior to that of a comparative cycle that uses R134a, CO2 systems can achieve superior efficiencies through specific cycle adjustments, such as two-stage compression, vapor injection, and inter-stage cooling.

1.3 Multisource heat pump

Multi-source heat pump were firstly introduced to obviate to the defects of a single source such as outside air, ground or solar radiation. The most common configurations in residential buildings are air-to-air or air-to-water: air-source heat pumps account for the majority of sales globally, with a market share of more than 60% in 2021.

Air, as a source, gives some design problem: air temperature is very variable during the heating months, when it decreases below 0°C the efficiency rapidly falls down also due to freezing of water that is present in the air on the evaporator’s wall. [18]

A very interesting configuration is to use a finned coil and a PVT (photovoltaic thermal) as evaporator in order to exploit both heat coming from the air and the solar radiation.

1.3.1 Photovoltaic-thermal (PVT)

PVT panels were firstly developed as a solution for the increasing temperature in photovoltaic panels during operation. As the temperature increases, due to the heat dissipated during the energy production, the open circuit voltage of module decreases. This lead to a decreasing power output. The PVT is used to produce electrical energy and thermal energy, in this way it is able to decrease the cells temperature achieving an higher efficiency of the panel. Chen et al. [19] built TRNSYS model of a PVT system (glazed and unglazed) and compared the year-round performance with a solar thermal collector and a photovoltaic system. The electrical efficiency values obtained for unglazed PVT, glazed PVT and photovoltaic are respectively 12.5%, 9.4% and 12.3%; while the average thermal efficiency values for the glazed PVT and the solar collector are 29.3% and 40%. The results showed that the use of PVTs provides a higher total production of photovoltaic and thermal energy.

In a PVT the main functional element is the heat absorber, as it transfers the solar energy collected by the photovoltaic cells to the fluid. The plates are usually made of metallic material such as copper and aluminium, their thermal conductivity must be the greatest possible. The various types of absorbers differ according to the manufacturing techniques, which also determine the choice of material to be used and the configuration of the channel. The most commonly used plates are: plate and tube (sheet-and-tube), roll bond and box channel.

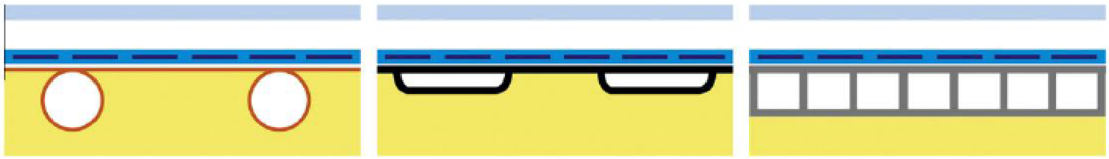

FIGURE(5) Heat absorber classification (sheet-and-tube; roll bond; box channel)

The first configuration (sheet metal and tube) consists of a flat plate to which channels with a circular section are generally welded or glued. The small contact surface between plate and pipe reduce significantly the heat transfer coefficient between the panel and the absorber. The roll bond configuration consists of joining two aluminium sheets by hot or cold rolling. This configuration gives a larger contact surface and the flexibility to design the channel, the main disadvantage is due to the impossibility , in the manufacturing process, to make plates with a thickness lower than 1mm. The last configuration, box channel, consists of parallel ducts with a rectangular section which form the plate, the advantage of this configuration is a larger contact surface between the plate and the channel, but special connectors are needed to joint the channel.

The low temperature thermal requirement of a heat pump makes it an excellent match for the use of solar energy. The concept of direct expansion solar-assisted heat pump (DX-SAHP) was first proposed in an experimental study by Sporn and Ambrose in 1955 [20], they used a double glazed collector that also act as evaporator in a R12 heat pump. In this study it was the first time that two-phase flow in collectors where considered but it didn’t demonstrate the full potential of the concept. Myngyan Zhu et al.[21] conduct a research on direct expansion solar assisted heat pumps (DX-SAHP)and analysed with three different type of collector: a bare-plate collector, a glass plate collector and a double collector evaporator. They concluded that under the similar external conditions the bare-plate collector system gives higher COP with higher irradiation and temperatures. Increasing the surface area led to an increasing COP but the collector efficiency decreases due to an increase of power demand at the compressor. With higher irradiance the water temperature rise rate will accelerate, the COP increases and the evaporation pressure will rise, but also the suction superheat will increase. In their article they demonstrated that a key point to improve the direct expansion type solar heat pump is the control of superheating. Emmanuel Bisengimana et al. [22]investigates the use of PVT for hot water and feeding a heat pump for building heating and cooling in Chengdu, Sichuan, China, over the course of a year. The system includes a PVT collector providing domestic hot water and electricity to run the heat pump and other appliances and light for a building with three rooms. This system was simulated using TRNSYS software, and the solar fractions of different months with different sizes of the PVT collector .Their results show that the solar intensity in Chengdu is not as favourable as other locations, which affects the energy generated by the PVT module. The study also shows that the solar electrical fraction increases significantly with an increase in PVT size, while the solar thermal fraction increases until it reaches 0.58, after which it shows a slight increase with an increase in PVT size. Emmi et al. [23] examine a Solar Assisted Ground Source Heat

Pump system. A dynamic simulations in TRNSYS environment is used to analyse both types of solar energy harvesting devices: solar thermal technology and the emerging photovoltaic thermal technology. The research demonstrates the potential to utilize solar energy directly for generating domestic hot water and as a heat source for a heat pump. The analysis reveals that using photovoltaic thermal panels can lead to a significant improvement in the efficiency of the heat pump.

1.4 Multisource heat pump and PVT

Heat pumps have the ability to use different sources other than air, such as ground heat, solar heat, and heat recovery, to enhance their performance. A multi-source system is designed to improve heat pump efficiency, resulting in substantial primary energy savings. Here some example of multi-source heat pumps.

Busato et al. [24] presented in their study 12 months of data monitoring and analysis from a real application in northern Italy. The energy balance demonstrates that integrating multiple sources not only boosts the overall thermal performance of the system, but also optimizes the use of each individual source.

Silvia Cesari et al. [25]presents in their project a novel heat pump-driven multi-source for the building climatization that can exploit sun, air and/or ground as thermal sources through the use of photovoltaic thermal solar panels, air heat exchangers and ground flat-panel heat exchanger. They demonstrate that using multiple renewable energy sources is a promising solution because it allows the heat pump to be supplied with the source that provides the most favourable temperature increase at any given time. However, over the course of a year and across seasons, this system would greatly benefit from proper thermal energy storage, which can be challenging to achieve. Nelson Sommerfeld et al. [26] in their study examines the technical and economic performance of ground source heat pump (GSHP) systems connected in series with solar PV/thermal (PVT) collectors in the context of multi-family houses (MFH) located in Sweden (heating-dominated climate). Using TRNSYS to simulate the system operation for 20 years, they calculate the system efficiency and lifecycle costs. The results show that PVT can reduce borehole length by 18% or spacing by 50% without compromising the seasonal performance factor of systems lacking PVT. Although PVT+GSHP systems are more costly than traditionally designed PV+GSHP, but this analysis does not consider the value of the land area saved by PVT, which can be as high as 89%. The reduction in land use made possible by PVT could help to increase the adoption of GSHP in MFH and promote the diffusion of solar energy in high latitude markets. Yifeng Wang et al. [27] proposed in their study an integrated ground source heat pump-photovoltaic-thermal (GSHP-PVT) system is proposed to provide combined clean heating/cooling, reduce heat transfer irreversible loss, and increase system flexibility by introducing double-evaporators with different working fluids. The system has five proposed operation modes for heating or cooling during the day or night in different seasons throughout the year. They generate different models for each modes in order to optimize the functioning of the system. The optimized results show that the COP of the GSHP-PVT system remains between 4 and 6 throughout the year. The proposed system operates with high efficiency preventing a decrease in the ground source temperature.

The utilization of multi-source heat pumps raises the issue of how to manage the selection of various thermal sources based on environmental conditions, thermal load, and storage. To address this problem, numerical tools can be helpful in evaluating the performance of multi-source heat pumps and determining a source selection strategy. For instance, Chargui et al. [28] simulated a dual-source heat pump using air and ground as heat sources and CO2 as the refrigerant with TRNSYS. The heat pump had two evaporators: one for heat exchange with a water source (solar or geothermal) and one for heat exchange with ambient air. In another study, Ma et al. [29] assessed the performance of indirect-expansion SAHPs using CO2 as the refrigerant for different configurations (one-stage and two-stage transcritical cycles) with TRNSYS models. They considered solar thermal collector area, storage tank volume, and heat pump compressor capacity and evaluated the performance variation.

Based on the reviewed literature, it appears that there is a shortage of research on PVT evaporators that operate with CO2, as well as numerical models that account for the entire direct-expansion heat pump system and its connection with the user water loop. To address these gaps, the present study seeks to investigate a direct-expansion dual source CO2 heat pump through both experimental and numerical means.

The main novelties are the followings:

- experimental tests conducted in dynamic conditions tests are presented when the heat pump operates in air and solar modes under real environmental conditions;
- a dynamic heat pump and water loop model has been developed using TRNSYS. The developed heat pump TRNSYS component includes the PV-T collectors mode;
- the dynamic model has been validated against the experimental data and it can be considered as an important tool to assess the heat pump performance over long-time and to develop a control strategy to maximize the advantages of a dual-source system.
- A new simulation with weather input data in Venice from the 1sr of January to the 15th of April is added. The analysis is taken both with the PVT and the finned coil in operation.

2 Heat pump prototype

In this paragraph the dual source heat pump prototype, object of this work of thesis is presented. This machine is installed at the University of Padova, Italy (45° 24′ 23″ N, 11° 52 40″ E), CO_2 has been chosen as working fluid and a transcritical cycle is performed. The main purpose is to produce DHW at the gas cooler.

The prototype has a nominal heating capacity of 5kW and has been designed to work with two evaporators a finned coil air heat exchanger or 3 photovoltaic thermal (PVT) solar collectors.

2.1 Cycle explanation

The layout of the system with the sensors installed and the auxiliary water loops is shown in Figure(6), and a simplified version of the p-h diagram is presented in Figure(7). Considering the refrigerant cycle after the inverter-driven rotary compressor (COMP), the high-pressure superheated refrigerant in the heat pump's refrigerant cycle is directed to the gas-cooler (GC). This is a brazed plate heat exchanger that employs counter-current water flow. Following the gas-cooler, the refrigerant flows into an internal heat exchanger (INT), where the CO2 is cooled. The refrigerant is then expanded through an electronic expansion device (EEV), which functions as a back-pressure valve regulating the gas-cooler pressure. At this point, the refrigerant can evaporate either inside the finned coil heat exchanger or within the solar PVT collectors. After the evaporation process, the CO2 enters the low-pressure receiver tank (REC), where the vapor phase is extracted from the top and sent to the compressor through the internal heat exchanger. This internal heat exchanger (INT) ensures some degree of superheating at the compressor suction. During heat pump operation, the high-pressure value on the gas-cooler side, the compressor speed, and the fan velocity at the finned coil evaporator can be controlled. It’s important to remember that an transcritical cycle is running, indeed at gas cooler no phase-change is occurred.

In the p-h diagram

1. Gas cooler outlet – expansion valve inlet
2. Expansion valve outlet - evaporator inlet
3. Evaporator outlet – Compressor inlet
4. Compressor outlet – gas cooler inlet

Points 1-2-3-4 are substituted by 1’-2’-3’-4’ when the internal heat exchanger is used. Here super heating of CO_2 vapour and subcooling of the liquid can be seen respectively in 3-3’ and 1-1’.

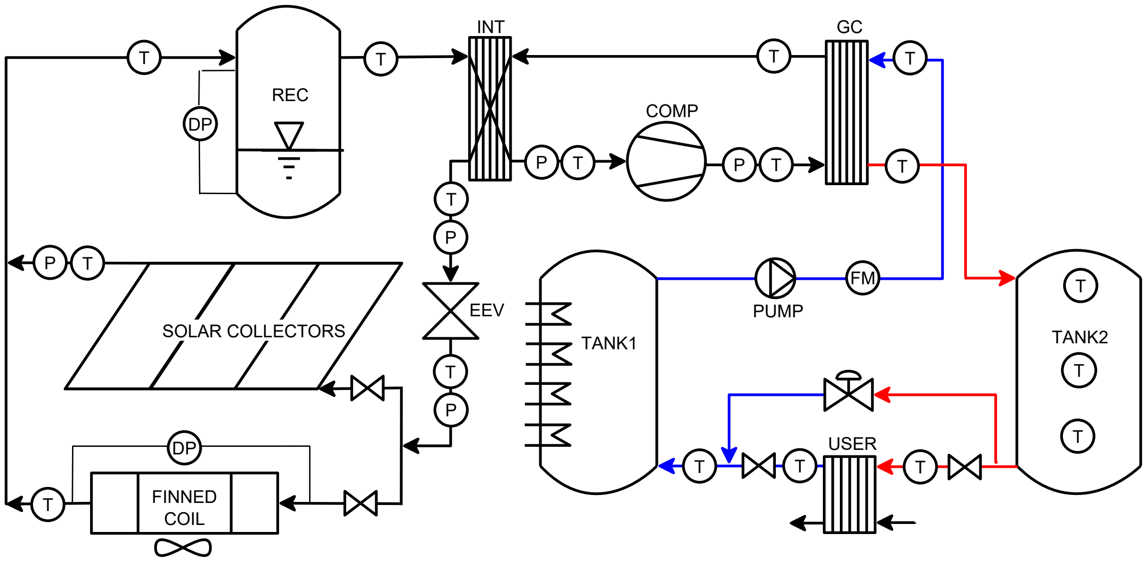
T
REC
DP
T
INT
T
GC
T
COMP
P
T
P
T
T
T
P
P
T
SOLAR COLLECTORS
EEV
T
P
TANK1
PUMP
FM
TANK2
T
T
T
DP
FINNED
COIL
T
USER
T
T
T

Figure (6) Layout of the heat pump and water loop with the sensors installed: T temperature probe, P pressure transducer, FM Coriolis flowmeter, DP differential pressure.

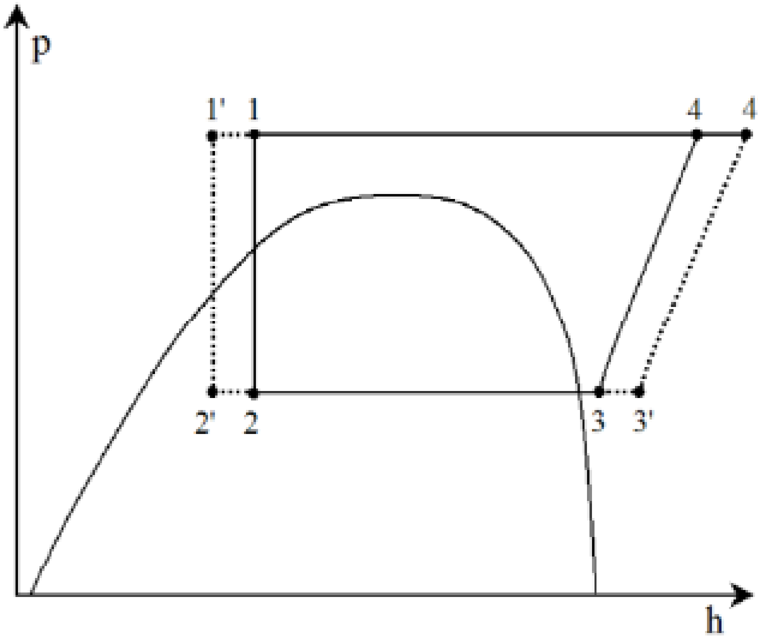

Figure(7) Heat pump cycle, p-h diagram

In Figure(8) the heat pump prototype casing, which houses the compressor, gas-cooler, internal heat exchanger, receiver, and expansion device, as well as the finned coil evaporator and the backs of three PVT collectors, are shown. In the water loop are installed two 200 L tanks and a brazed plate heat exchanger (USER in Figure (6)) located between them. The cold tank, TANK1, releases water that is pumped to the gas-cooler. The water is then heated in the gas-cooler and transferred to the hot tank, TANK2. The USER plate heat exchanger is used to simulate the user's heat flow rate request. A by-pass valve modulates the mass flow rate in the USER heat exchanger. Two valves located before and after the USER heat exchanger allow this part of the circuit to be isolated when there is no thermal load request by the user. The temperature at the gas-cooler inlet was maintained at approximately 30°C during the experimental campaign, and the TANK1 temperature was controlled by four variable electrical resistances capable of producing up to 4.5 kW each. Figure(9) depicts a picture of the water loop with the two tanks and the USER brazed plate heat exchanger. The refrigerant circuit and water loop are insulated to limit heat losses to the external ambient.

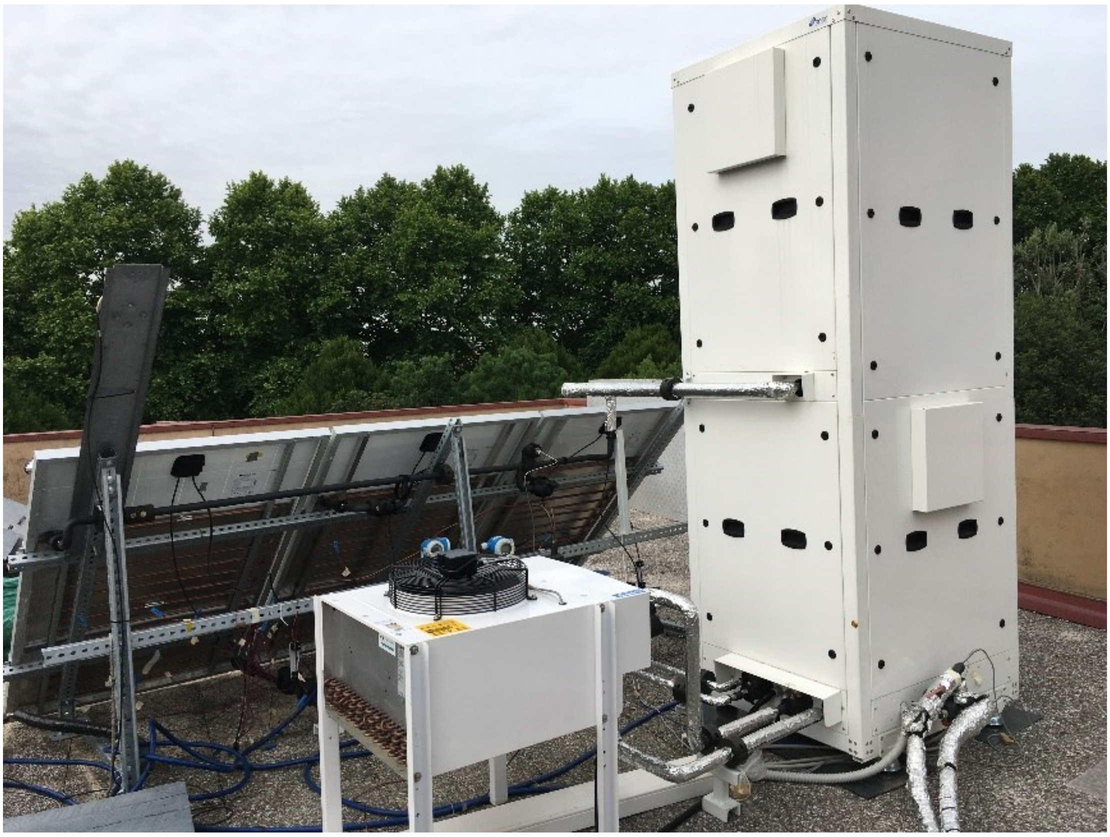

Figure (8)Picture of the heat pump prototype, including finned coil evaporator and PVT collectors.

Figure(9) Picture of the water tanks and the USER brazed plate heat exchanger.

2.2.Heat exchanger

In heat pumps the heat exchangers play a very important role in the operation of the "refrigerant cycle". In this prototype there are 4 heat exchangers:

1. In air-mode, a conventional finned coil heat exchanger with 22 ranks and 4 rows is used as the evaporator. The fluid flow is split into 4 circuits consisting of 3.2 mm internal diameter tubes. The finned coil evaporator is connected to a fan, which is modulated by a 0-10 Vdc signal to adjust its rotation speed.
2. In solar-mode, three PVT solar collectors are used as the evaporator. Using a PVT device offers two advantages, as seen before: it enables the energy from solar radiation to evaporate the refrigerant flow, and improves the PV electricity conversion by cooling the photovoltaic cells. Each PVT collector has an aluminum plate (0.5 mm thickness) glued beneath a multicrystalline PV module. An 8 mm external diameter copper serpentine is coupled with each plate. The PV modules are connected to a variable electrical resistance that enables them to operate at the maximum power point (MPPT). Table 1 lists the primary characteristics of the PVT collectors

3. The gas-cooler is a brazed plate heat exchanger, where water and CO2 flow in a single pass/counter-current configuration. It comprises 28 plates with external dimensions of 379 x 79 mm.
4. An internal heat exchanger is used to increase the temperature of the vapor CO2 exiting the low-pressure receiver. This is achieved by further cooling the CO2 that exits the gas-cooler. The internal heat exchanger is a brazed plate heat exchanger with 4 plates in a single pass/counter-current configuration. The external dimensions of the plates are 377 x 120 mm.

Table(2) Main characteristic of the PVT collector.

Dimensions	1650 x 992 mm
Tilt angle	45°
Absorber thickness	0.5 mm
Tube thickness	1 mm
External tube diameter	8 mm
Tube pitch	80 mm
Number of tubes	15

Table (2) PVT characteristics

2.3.Data collection

Multiple sensors have been installed in the heat pump and water circuit systems (refer to Figure 1). For the heat pump, T-type thermocouples and pressure transducers have been placed at the inlet and outlet of each component. To evaluate the pressure drop inside the finned coil heat exchanger, one differential pressure transducer has been used. The air temperature has been assessed using a PT-100 resistance temperature detector and solar irradiance on the tilt angle of the PVT collectors has been evaluated using a secondary standard pyranometer. Wind velocity has been measured using a cup anemometer. The power analyzer Norma 4000 has been used to measure compressor power consumption (including inverter), global power consumption of the heat pump, and power produced by photovoltaic modules.

For the water loop, a Coriolis effect mass flow meter has been used to measure water mass flow rate, while two PT-100s inside thermowells have been used to measure water temperatures at the inlet and outlet of the gas-cooler. To evaluate the water thermal stratification in the TANK2, three thermocouples have been placed in thermowells at different heights, and two thermocouples have been used to measure water temperature at the inlet and outlet of the USER heat exchanger, with one thermocouple to measure the water temperature before entering TANK1.

The energy balance on the water-side can be used to calculate the heating capacity produced at the gas-cooler, where water mass flow rate measured by the Coriolis flowmeter ($\dot{m}_w$), water specific heat capacity (c_p), and the difference between the water temperatures measured at the outlet and inlet of the gas-cooler $T_{out_{gc},w}$ - $T_{in_{gc},w}$ are used.

$$Q_{gc}=\dot{m}_w \cdot c_p \cdot \left(T_{out_{gc},w}-T_{in_{gc},w}\right) \tag{1}$$

To calculate the heat flow rate delivered to the user, assuming the USER heat exchanger and bypass line as a black box, the difference between the temperature measured at the inlet of the USER heat exchanger (i.e. at the outlet of TANK2) and the temperature measured before entering TANK1 is used.

$$Q_{user}=\dot{m}_w \cdot c_p \cdot \left(T_{out_{T2}}-T_{in_{T1}}\right) \tag{2}$$

All data is continuously recorded by a data logger Agilent 34970 with a time step of 10 seconds, while the uncertainties of the sensors are reported in Table(3) All this data were collected in previous works [30], [31].

Parameter	Sensor Type	Uncertainty
Temperature	T-type thermocouples	±0.1 K
Temperature	PT-100 resistance temperature detector	1/10 DIN
Pressure	Pressure transducers	±5 kPa
Solar irradiance	Secondary standard pyranometer	ISO 9060
Water mass flow rate	Coriolis effect flow meter	0.1% of the reading
Electric power	Power analyzer Norma 4000	0.1% of the reading

Table(3) Uncertainty of sensors used

3 Numerical model

All simulations have been developed in TRNSYS 17, a flexible graphically based software environment used to simulate the behavior of transient systems.

3.1 Heat pump model

To model the heat pump, a TRNSYS type (named HP) was created based on the heat pump type described by Zarrella et al. in [32] and Scotton in [33]. These two works have been adapted to the actual heat pump prototype. The numerical model uses an iterative algorithm to solve the supercritical carbon dioxide cycle under various external conditions and operative modes. The base algorithm was presented in Zanetti et al. [31], but a novel approach was used in the numerical tool described in this work to model the gas cooler and PVT collectors . In this work, the TRNSYS component proposed by Zarrella et al. [32] was developed to model the PVT collectors as the evaporator of the heat pump, and was integrated into the model of the heat pump. The HP type can determine the heat pump's energy fluxes and performance indicators based on environmental conditions, compressor speed, and high-pressure value. The model simulates the steady-state operation of the unit, as its transient operation is negligible compared to the inertia of the water storage tanks.

The following assumption have been made:

- The pressure drop in the heat exchangers is neglected.
- the heat exchangers and compressor are adiabatic.
- The high-pressure value is a model input, as it can be selected through the back-pressure expansion device.

The Refprop subroutine is used to calculate the intermediate fluid properties in the model. The refrigerant cycle solution algorithm is implemented in the following steps (Zanetti et al. [30]):

- Assume tentative values of the evaporation temperature and pressure based on the environmental conditions. As demonstrated by Zanetti et al. [30], in the present heat pump prototype, the CO_2 exits the evaporators as saturated vapor (vapor quality between 0.94 and 1) in any operating condition. Therefore, in the model the vapor quality at the evaporator outlet is fixed equal to 1 and the enthalpy $h_{out,e}$ can be calculated as a function of the evaporation temperature.

- Calculate the refrigerant mass flow rate, compressor power consumption, and specific compressor work with a 20-coefficient polynomial of three degrees, depending on the evaporation temperature, the pressure at the gas-cooler, and the compressor speed; [30]
- Calculate the refrigerant temperature at the gas-cooler outlet $T_{out_{gc},r}$ through the gas-cooler model; [34]
- Solve the energy balance at the internal heat exchanger with the mean logarithmic temperature difference method:

$$Q_{int}=(KA)_{int}\frac{\left(T_{out_{gc},r}-T_{in,c}\right)-\left(T_{in,lam}-T_{out,e}\right)}{\log\left(\frac{T_{out_{gc},r}-T_{in,c}}{T_{in,lam}-T_{out,e}}\right)} \tag{3}$$

- In Eq. 3 the overall heat transfer coefficient/exchange area product $(KA)_{int}$ has been derived from the experimental data in a linear equation as a function of the refrigerant mass flow rate:

$$(KA)_{int} = 1011.6 \cdot \dot{m}_r - 2.1987 \tag{4}$$

- An updated value of the refrigerant conditions at the outlet of the internal heat exchanger ($h_{in,lam}$) can thus be calculated:

$$h_{in,lam}=h_{out,lam} + \frac{Q_{int}}{\dot{m}_r} \tag{5}$$

- The enthalpy at the inlet of the evaporator is considered to be equal to the enthalpy at the EEV inlet (isenthalpic expansion)

- An updated value of the evaporation temperature is finally obtained, based on the used evaporator and the environmental conditions.

- The procedure is repeated until the evaporation temperature reaches a convergence value within a tolerance of 0.01 K. When considering solar-mode operations, the temperature of all the nodes should converge within the fixed tolerance value.

3.2 PVT model

The PVT panels in this study were modeled using a lumped parameter approach which represents each layer of the PVT collector as a thermal node. The model is based on heat balance equations, which are used to calculate the temperature of each node and derive the electrical and thermal performance of the PVT collector. The PVT panel consists of three main layers:

(1) the protective upper glass
(2) the PV layer
(3) and the absorber plate.

The fluid node is added to the resistance system that corresponds to these layers. The model accounts for conduction, convection, and radiation heat fluxes within the different layers of the panel, as well as the external ambient conditions.

The thermal capacitance of the different nodes is neglected in the model. This lumped parameter approach is a simplified method to model the PVT collector's performance and may not capture all the intricacies of the physical system. Nonetheless, this model was validated in a previous study [32] and is used in this work to evaluate the performance of the PVT panels when integrated into a heat pump system.

The PVT panels model was integrated into the heat pump's model for use in the TRNSYS type. The integration of the PVT panel model with the heat pump model allows for the analysis of the combined performance of the PVT panels and heat pump system.

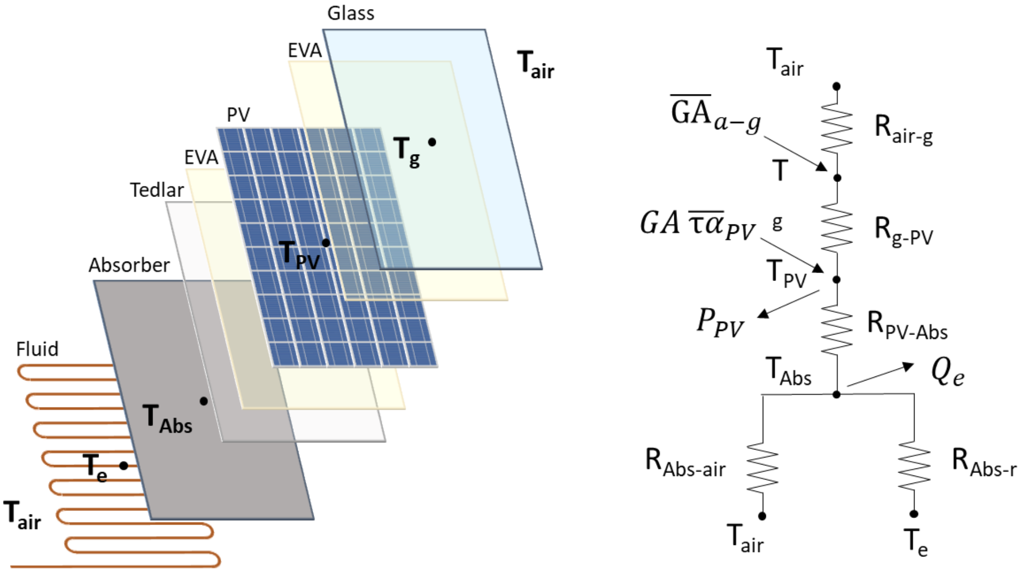
Glass
EVA
T_{air}
PV
T_g
EVA
Tedlar
T_{PV}
Absorber
Fluid
T_{Abs}
T_e
T_{air}
T_{air}
$\overline{GA}_{a-g}$
R_{air-g}
T
g
$GA\,\overline{\tau\alpha}_{PV}$
R_{g-PV}
T_{PV}
P_{PV}
R_{PV-Abs}
T_{Abs}
Q_e
$R_{Abs-air}$
R_{Abs-r}
T_{air}
T_e

(a) (b)

Figure(8) (a) Section of the PVT model and (b) Scheme of the equivalent electrical network of the PVT model

The model takes in various inputs such as:

- the incident solar radiation
- the angle at which the beam radiation hits
- external air and sky temperatures
- wind velocity
- the refrigerant temperature and flow rate at the inlet

The outputs include:

- the thermal and electrical power produced by the PVT panel
- the outlet refrigerant temperature
- the average temperature of each thermal node.

To obtain the incident solar radiation on the PV layer, the model accounts for refraction, absorption, and reflection phenomena and solves a system of equations for each node of the 1-D network of thermal resistances, using the same method as described in [32]. The heat balance equations for different nodes are also calculated by the model as follows:

3.2.1 The energy balance on the glass node

The first node of the equivalent electrical network represented in Figure(8) is the glass node. The unknown variables in the energy balance equation (Eq. 6) are the temperatures T_g and T_{PV}. The first term of the equation is the net solar radiation absorbed by the glass, defined in Eq. (7). In Eq. (7), α_g is the global coefficient of absorption of the glass, ρ_g is the global coefficient of reflection of the glass and $\overline{\tau\alpha}_{PV}$ is the ratio of absorbed solar radiation by the PV cells (Eq. 10). The thermal resistance R_{g-PV} (Eq. 8) depends on the geometry (thickness) and thermal properties (thermal conductivity) of the materials composing the considered layers. H_{g-air} (Eq. 9) is the global transmission coefficient on the glass surface, where ϵ_g is the glass emittance, σ is the Stefan-Boltzmann constant, β is the slope of the PVT panel surface and v is the wind velocity.

$$\overline{GA}_{a-g} + A \cdot \frac{T_{PV}-T_g}{R_{g-PV}} - A \cdot \left(T_g - T_{air}\right) \cdot H_{g-air} = 0 \tag{6}$$

$$\overline{GA}_{a-g} = G \cdot A \cdot \alpha_g + G \cdot A \cdot \left(1 - \alpha_g - \rho_g - \overline{\tau\alpha}_{PV}\right) \cdot \alpha_g \tag{73}$$

$$R_{g-PV} = \frac{t_g}{2 \cdot \lambda_g} + \frac{t_{EVA}}{\lambda_{EVA}} + \frac{t_{PV}}{2 \cdot \lambda_{PV}} \tag{8}$$

$$H_{g-air} = \epsilon_g \cdot \sigma \cdot \frac{T_g^4 - T_{sky}^4}{T_g - T_{air}} + 1.247 \cdot \left[\left(T_g - T_{air}\right) \cdot \cos\beta\right]^{\frac{1}{3}} + 2.658 \cdot v \tag{9}$$

$$\overline{\tau\alpha}_{PV} = \frac{\tau_g \cdot \alpha_{PV}}{1 - \rho_d \cdot (1 - \alpha_{PV})} \tag{10}$$

3.2.2 The energy balance of the PV node

The energy balance of the PV cell layer is shown in Eq. (11). The thermal resistance R_{PV-Abs} between the PV layer and the absorber plate is a function of the geometry of the system and the thermal properties of the materials (Eq. (12)). The last term represents the energy flux converted into electrical power by the PV system (Eq. (13)). The values of the coefficients η_{PV} and T_{ref-PV} can be found in the PV or PVT panel datasheet and represent the reference efficiency of the PV module at the reference temperature T_{ref-PV}. The value of b_{PV} represents the deviation in efficiency from the reference values.

$$G \cdot A \cdot \overline{\tau\alpha}_{PV} - A \cdot \frac{(T_{PV} - T_g)}{R_{g-PV}} - A \cdot \frac{(T_{PV} - T_{Abs})}{R_{PV-Abs}} - P_{PV} = 0 \tag{11}$$

$$R_{PV-Abs} = \frac{t_{PV}}{2 \cdot \lambda_{PV}} + \frac{2 \cdot t_{EVA}}{\lambda_{EVA}} + \frac{t_{Tedlar}}{\lambda_{Tedlar}} + \frac{t_{Abs}}{2 \cdot \lambda_{Abs}} \tag{12}$$

$$P_{PV} = G \cdot A \cdot \eta_{PV} \cdot [1 - b_{PV} \cdot (T_{PV} - T_{ref-PV})] \tag{134}$$

3.2.3 The energy balance of the absorber plate node

Eq. (14) shows the energy balance of the absorber plate. The first two terms represent the heat exchanged with the PV layer and the air on the rear side of the panel (Eq. 15). The last term is the heat flow rate provided to the refrigerant and it is calculated with Eq. (16).

$$A \cdot \frac{T_{PV}-T_{Abs}}{R_{PV-Abs}} - A \cdot (T_{Abs} - T_{air}) \cdot H_{Abs-air} - Q_e = 0 \tag{14}$$

$$H_{Abs-air} = \epsilon_g \cdot \sigma \cdot \frac{T_{Abs}^4 - T_{sky}^4}{T_{Abs}-T_{air}} + 1.247 \cdot [(T_{Abs} - T_{air}) \cdot \cos\beta]^{\frac{1}{3}} + 2.658 \cdot v \tag{155}$$

3.2.4 The energy balance of the fluid node

Eq. (16) reports the energy balance equation for the fourth node. Q_e is the heat exchanged between the absorber and the refrigerant, and the second term includes the thermal resistance between the absorber plate and the refrigerant, computed as in Eq. (17).

In Eq. (17), D_{pipe} and l_{pipe} are the hydraulic diameter and the length of the channel, and K is the overall heat transfer coefficient of the pipe, with η_{fin} the fin efficiency. The heat transfer coefficient K_e is evaluated using Eq. (18), where the thermal resistance due to the welding (subscript "we"), the conduction thermal resistance due to the pipe thickness and the heat transfer coefficient between the fluid and the internal wall (htc_r) are considered. In this work, the value of htc_r is considered constant and equal to 280 W m^{-2} K^{-1}.

$$Q_e - \frac{T_{Abs}-T_e}{R_{Abs-r}} = 0 \tag{16}$$

$$R_{Abs-r} = \frac{4}{\pi \cdot D_{pipe} \cdot l_{pipe} \cdot K_e \cdot \eta_{fin}} \tag{176}$$

$$K_e = \left(\frac{1}{htc_r} + \frac{t_{we}}{\lambda_{we}} + \frac{t_{pipe}}{\lambda_{pipe}}\right)^{-1} \tag{18}$$

The temperatures of the thermal nodes are monitored during two consecutive iterations to ensure the thermal equilibrium in each node is reached. Once the temperature difference between two successive iterations at each node ($\Delta T_{node\ n,i/i-1}$) is computed, the iteration process stops when the maximum $\Delta T_{node\ n,i/i-1}$ is lower than a set tolerance (i.e. 0.01 K).

A flow chart summarizing the main steps of the PVT model integrated in the heat pump model is shown in Figure(9)

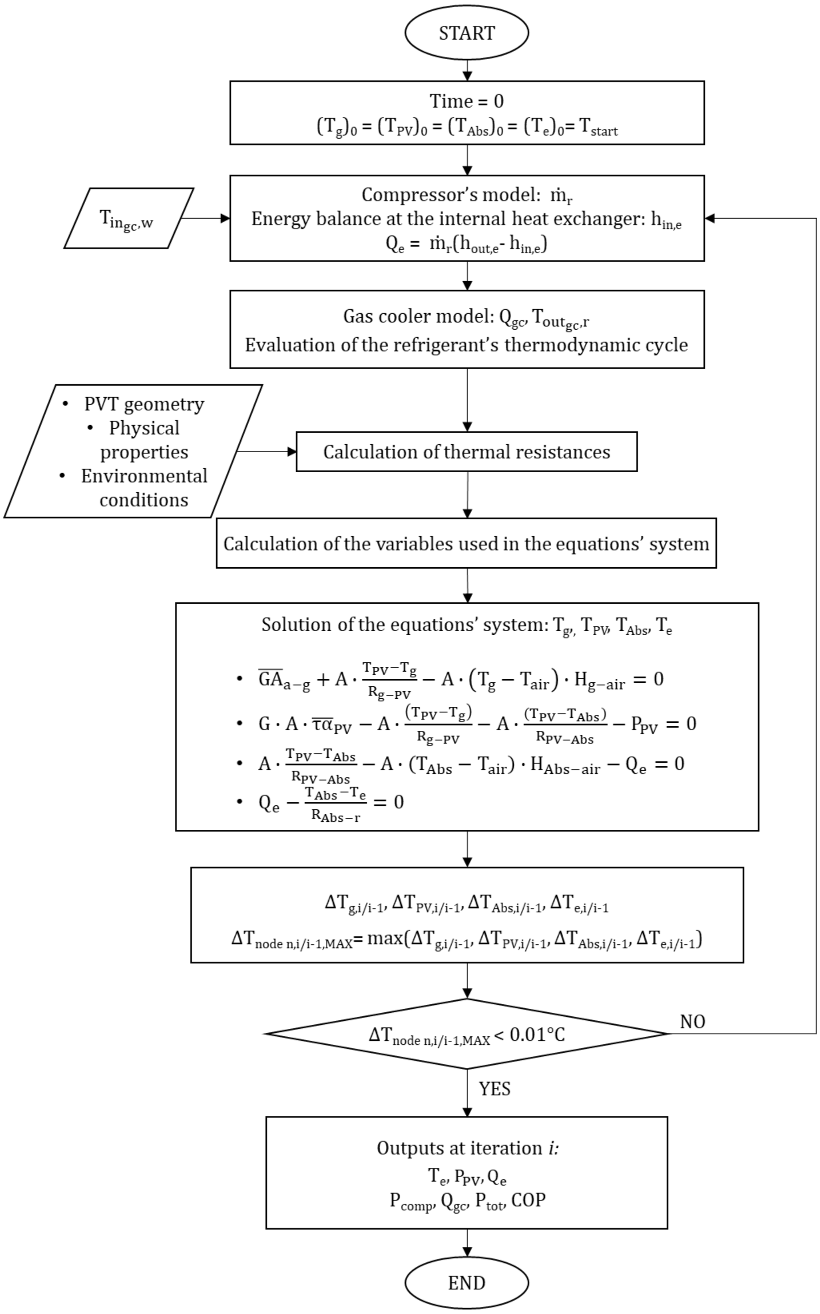
START
Time = 0
$(T_g)_0 = (T_{PV})_0 = (T_{Abs})_0 = (T_e)_0 = T_{start}$
$T_{in_{gc},w}$
Compressor's model: $\dot{m}_r$
Energy balance at the internal heat exchanger: $h_{in,e}$
$Q_e = \dot{m}_r(h_{out,e} - h_{in,e})$
Gas cooler model: Q_{gc}, $T_{out_{gc},r}$
Evaluation of the refrigerant's thermodynamic cycle
PVT geometry
Physical properties
Environmental conditions
Calculation of thermal resistances
Calculation of the variables used in the equations' system
Solution of the equations' system: T_g, T_{PV}, T_{Abs}, T_e
$\overline{GA}_{a-g} + A \cdot \frac{T_{PV}-T_g}{R_{g-PV}} - A \cdot (T_g - T_{air}) \cdot H_{g-air} = 0$
$G \cdot A \cdot \overline{\tau\alpha}_{PV} - A \cdot \frac{(T_{PV}-T_g)}{R_{g-PV}} - A \cdot \frac{(T_{PV}-T_{Abs})}{R_{PV-Abs}} - P_{PV} = 0$
$A \cdot \frac{T_{PV}-T_{Abs}}{R_{PV-Abs}} - A \cdot (T_{Abs} - T_{air}) \cdot H_{Abs-air} - Q_e = 0$
$Q_e - \frac{T_{Abs}-T_e}{R_{Abs-r}} = 0$
$\Delta T_{g,i/i-1}$, $\Delta T_{PV,i/i-1}$, $\Delta T_{Abs,i/i-1}$, $\Delta T_{e,i/i-1}$
$\Delta T_{node\ n,i/i-1,MAX} = \max(\Delta T_{g,i/i-1}, \Delta T_{PV,i/i-1}, \Delta T_{Abs,i/i-1}, \Delta T_{e,i/i-1})$
$\Delta T_{node\ n,i/i-1,MAX} < 0.01°C$
NO
YES
Outputs at iteration *i:*
T_e, P_{PV}, Q_e
P_{comp}, Q_{gc}, P_{tot}, COP
END

Figure(9) Flow chart of the PVT model integration in the heat pump model.

5 Heat pump - TRNSYS model

The system modelled in the TRNSYS environment and presented by Zanetti et al. in [34] is shown in Figure(10). The water loop of the system is highlighted in blue lines. The circulator pumps water, which is then warmed inside the gas-cooler of the heat pump. The water flow rate then enters TANK2 from the upper part, while the outlet of the thermal storage is located in the bottom part. A diverter is used to convey the water exiting from TANK2 directly to the mixing valve or to the plate heat exchanger to meet the USER thermal load. After passing through the mixing valve, the total water stream is directed to TANK1, and then the flow rate is delivered to the circulation pump, closing the loop.

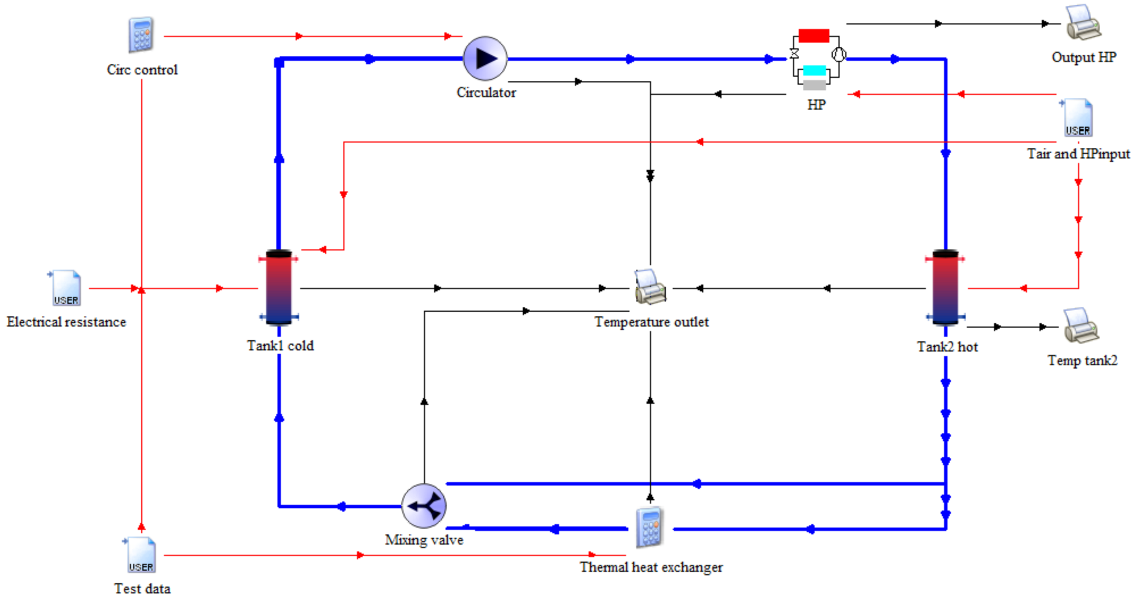
Circ control
Circulator
HP
Output HP
USER
Tair and HPinput
USER
Electrical resistance
Tank1 cold
Temperature outlet
Tank2 hot
Temp tank2
Mixing valve
Thermal heat exchanger
USER
Test data

Figure(10) Scheme of the system modelled in Simulation Studio (TRNSYS) [34]

In Figure(10) all the types used in the simulation are shown. A short explanation of each one is found in table(4)

Module name	**Module icon**	**Module introduction**
HP - Type 211	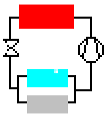	The mathematical model of the heat pump.
Tank - Type 534	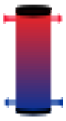	A water tank with electrical resistances used as auxiliary heaters.
Thermal heat exchanger		Calculator used to simulate the User heat request.
Mixing valve – Type 11h		Valve used to mix water coming from the hot tank and the thermal heat exchanger.
Circulator – Type 3d	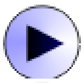	Pump model, controls the flow rate.
Printer – Type 25c		Generates TXT files according to output.
Data reader – Type 9e		Data reader with the input TXT files

Table(4) Type used in Simulation Studio

The inputs to the model are:

- the thermal load to be provided to the user;
- the heat exchanger inlet and outlet well water temperatures;
- the total water flow rate circulating in the system;
- the external air temperature;
- the supply voltage of the compressor, throttling valve and fan;
- the power of the electrical resistances in the TANK1.

The flow diverter and plate heat exchanger are simulated using simple equations. The flow rate delivered to the heat exchanger ($\dot{m}_{HE}$) is calculated using the real temperature difference of the well water between the inlet and the outlet of this component and the thermal load, measured during the experimental campaign.

$$\dot{m}_{HE}=\frac{Q_{user}}{c_p\cdot\left(T_{out_{T2_m}}-T_{out_{HE_m}}\right)} \tag{19}$$

where Q_{user} is the user's thermal load, $T_{out_{HE_m}}$ and $T_{out_{T2_m}}$ are the temperatures at the outlet of the USER heat exchanger and the TANK2, respectively.

Once the mass flow rate value through the heat exchanger is computed, the temperature at the outlet of the heat exchanger is calculated using the modelled temperature at the inlet.

$$T_{out_{HE_s}}=T_{out_{T2_s}}-\left(\frac{Q_{user}}{c_p\cdot\dot{m}_{HE}}\right) \tag{20}$$

Here $T_{out_{T2_s}}$ is the temperature at the outlet of TANK2 calculated by the model.

5.1 Experimental test

Experimental tests were conducted under transient conditions to simulate variable thermal loads on the user heat exchanger in real environmental conditions. Each test had a duration of 6 hours and was carried out based on the following conditions:

1. The user was provided with water at a temperature not lower than 45°C while monitoring the thermocouple at the bottom of TANK2 ,as depicted in Figure 1.
2. The heat pump was activated when the water temperature, measured by the thermocouple in the middle of TANK2, dropped below 50°C. This was done to ensure compliance with condition 1, taking into account system inertia and the necessary time for the compressor to reach maximum speed.
3. The heat pump was turned off when the thermocouple located at the half-height of TANK2 recorded a temperature of 55°C.
4. During air-mode, the compressor was operated at maximum speed, while the fan of the finned coil heat exchanger was run at the highest velocity. The compressor speed was set to 75% of full speed in solar-mode.
5. The gas-cooler inlet water temperature was maintained between 27°C to 31°C. When necessary, the temperature in TANK1 was regulated by turning the electrical resistances on or off.
6. The electronic expansion valve, which acted as a back-pressure valve, automatically regulated the high pressure to be equal to or higher than 95 bar. The maximum pressure was 100 bar**.**

5.1.1 Finned coil test

Figures (11) and (12) report the user thermal load (Q_user), heating capacity (Q_gc), and water flow rate (fr_w) during two intervals of the same test day when the heat pump was in air-mode and the ambient temperature was between 9°C and 11°C.

Figure(11) displays the experimental results when the heat pump was turned on (at time 15:36) to fulfill condition 2. The heat pump took 5 minutes to reach maximum heating capacity. This operative condition allowed for the presence of both Q_user and Q_gc at the same time. The maximum water flow rate was 400 L/h, while the minimum stable value was 80 L/h. The maximum heating capacity was 5 kW (excluding peak values resulting from sudden changes in water flow rate), while the maximum user thermal load was 8 kW with the heat pump off or 7 kW with the heat pump on. At 15:50 and 16:30, the USER heat exchanger was isolated for a few minutes by closing the relevant valves to simulate a no-user load condition. However, the heat pump continued to operate because the temperature in TANK2 did not satisfy condition c3.

Figure(12) presents an experimental test with a continuous thermal load request from the user while the heat pump was off from 13:35 to 13:50 due to condition c6 being met. The water flow rate ranged from 80 L/h to 260 L/h, the maximum heating capacity was 5 kW, and the maximum user thermal load was approximately 7 kW. The heat pump took about 1 minute to turn off. These two tests show that changes in the water flow rate have a greater impact on the user thermal load than the heating capacity, owing to the single loop of the water circuit.

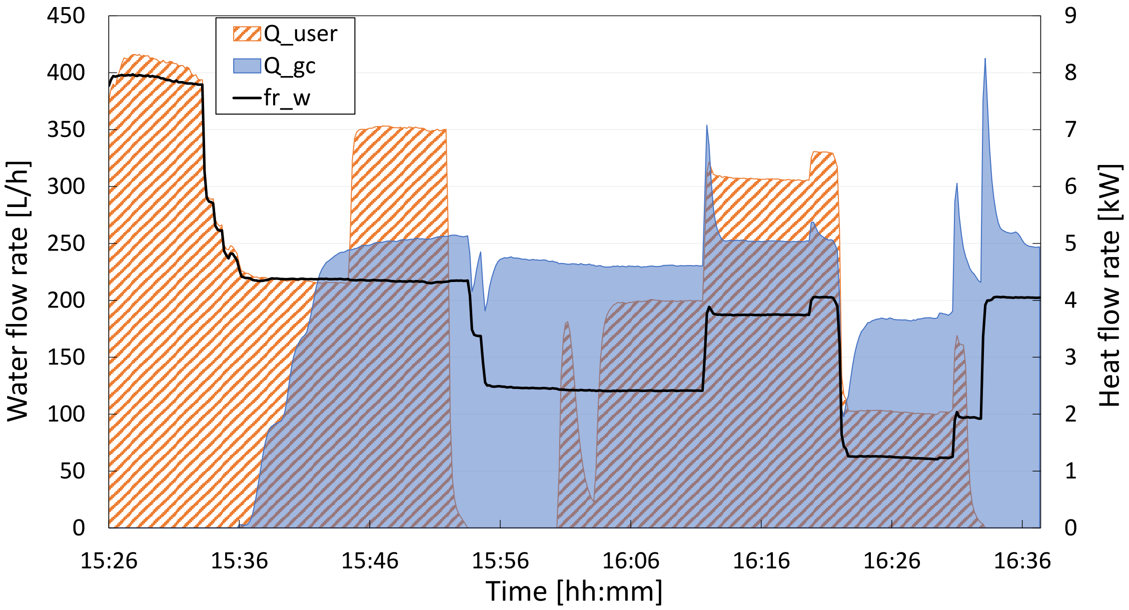

Figure(11) User thermal load, heating capacity, and water flow rate during the experimental test with finned coil evaporator. [34]

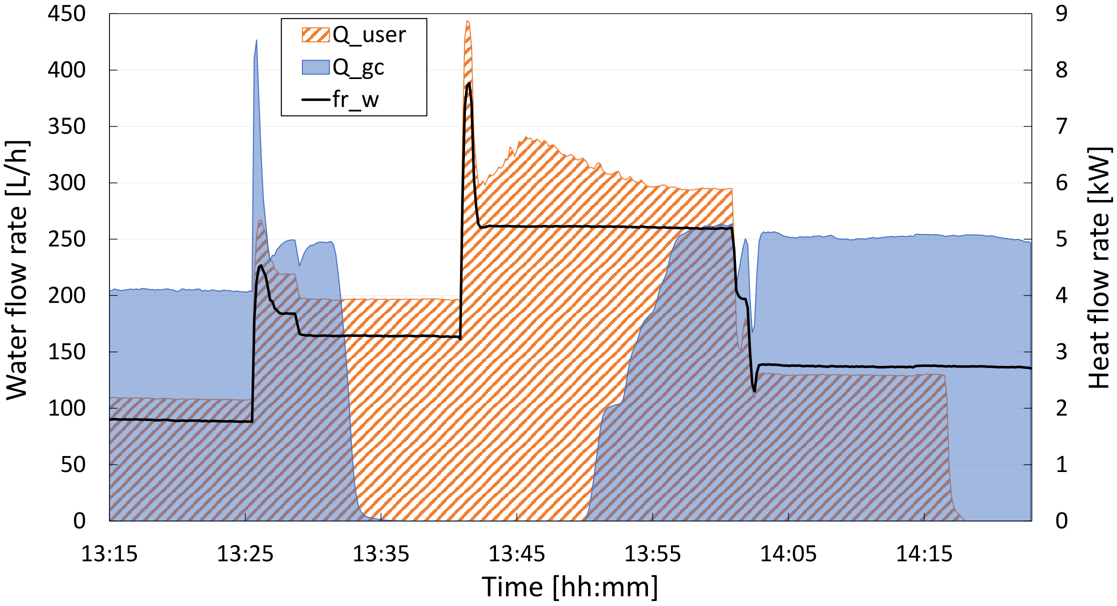

Figure(12) User thermal load, heating capacity and water flow rate during the experimental test with finned coil evaporator. [34]

5.1.2 PVT test

The experimental test in Figure(13) utilizes PVT collectors as the evaporator and displays the user's thermal load, heating capacity, and water flow rate. The test ranges from a water flow rate of 66 L/h to 180 L/h, with a maximum heating capacity of 3 kW and a maximum user thermal load of 6 kW. The heating capacity produced at the gas-cooler is reduced in comparison to the air-mode tests, as the compressor speed has been fixed at 75% of the maximum speed (reported in condition c4). It takes 5 minutes for the heat pump to reach a constant value of heating capacity, similar to the air-mode tests.

Figure(14) demonstrates the photovoltaic power production (P_PV) and global tilted irradiance (GTI) during the test. At the start of the test, with the heat pump off, the power production was 750 W. Upon the heat pump's switch-on, the photovoltaic power production increased to 810 W (about +8%) due to the cooling effect of the refrigerant evaporating in the sheet and tube heat exchangers coupled to the PV panels.

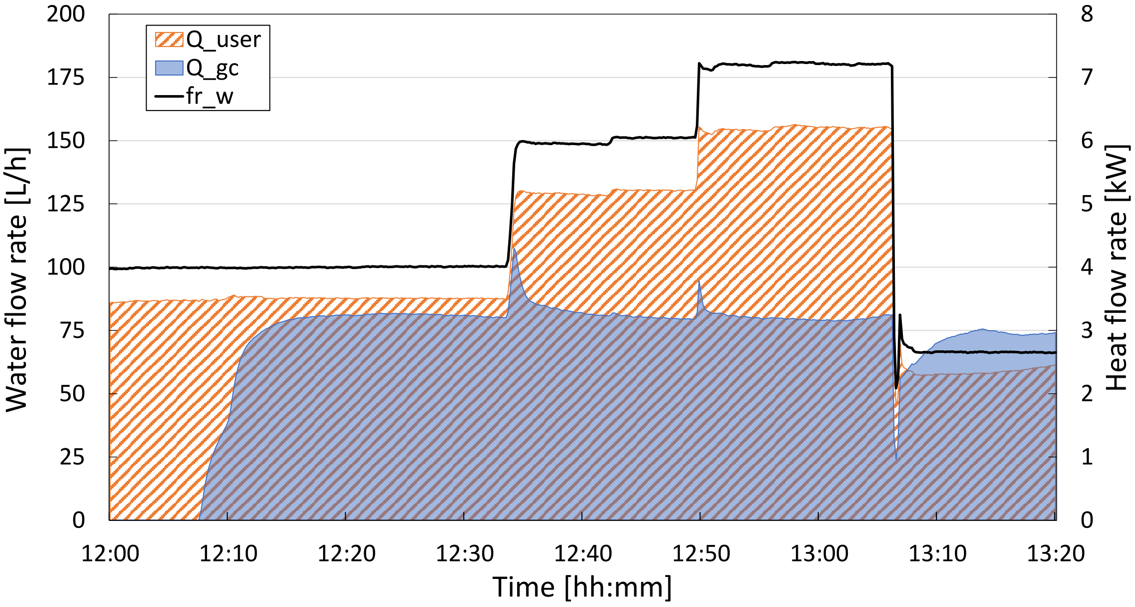

Figure (13) User thermal load, heating capacity and water mass flow rate during the experimental test with PVT collectors. [34]

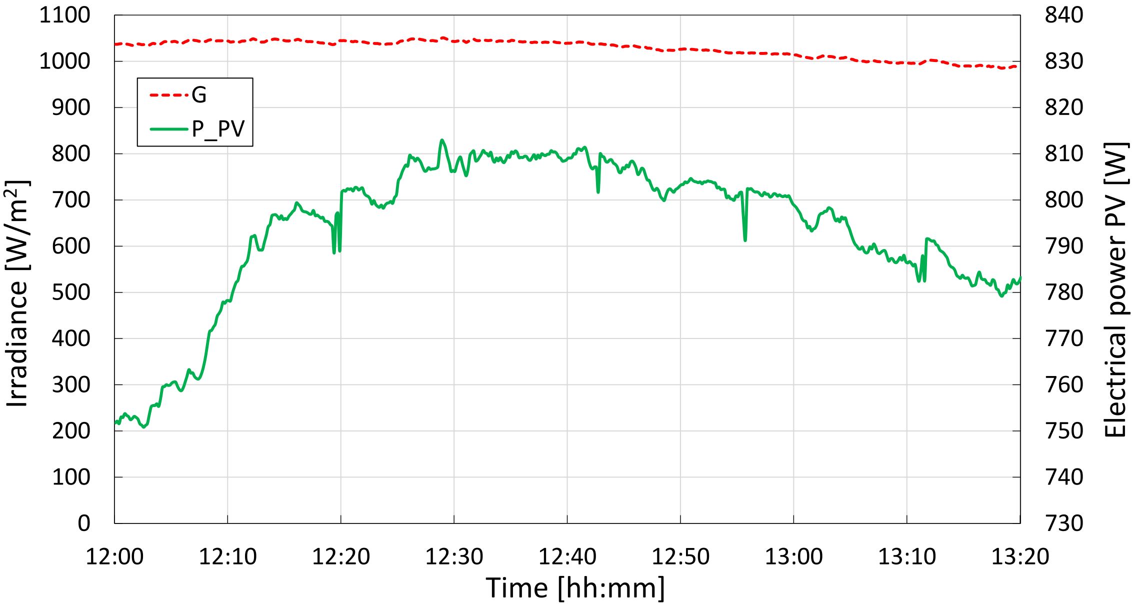

Figure(14) Global Tilted Irradiance (G) and photovoltaic power production (P_PV) during the experimental test with PVT collectors. [34]

5.2 Model validation

In this paragraph, a comparison between the measurements and the results obtained from the TRNSYS model (Zanetti et al. [34]) is presented and discussed. The model's plant has been preliminarily calibrated using data from a monitoring campaign. The calibration involved adjusting some of the tanks' parameters, such as the number of isothermal nodes used to subdivide the two storages and the position of the inlet and outlet nodes. This choice of modulization impacts the simulation of fluid stratification within the storage and its temperature at the outlet. The best parameters were selected based on the root mean square error (RMSE) of the water temperature at the outlet of the two tanks. The optimal results were obtained by dividing TANK1 into nine nodes and TANK2 into twelve nodes, with nodes numbered from the upper part of the 1.4 m high thermal storages. In the model, Node 8 of TANK1 is where the inlet port is located, while the outlet port is at Node 1. Similarly, in TANK2, the inlet port is at node 2, and the outlet port is at node 12. With these assumptions for the case where the finned coil is used as the evaporator, an RMSE of 7.2% for TANK1 and 3.6% for TANK2 was obtained.

5.2.1 PVT validation

The PVT model described was firstly validated using data collected from the heat pump prototype on different days. In this analysis, only the heat pump running with the PVT is simulated.

The input data are:

1. GTI: solar irradiance [W/m^2]
2. Θ: Incidence angle on the tilted surface [°]
3. T_{air}: Air temperature [°C]
4. v_{wind}: Wind velocity in [m/s]
5. V_{comp}: Voltage applied to the compressor, the higher the voltage the higher the velocity of the compressor [V]
6. V_{valv}: Voltage applied to the expansion valve, the higher the voltage the higher the valve opening[V]
7. Fr_{water}: water flow rate [kg/s]

In the following table the input data used for the validation are reported. They are ordered with increasing compressor velocity and valve opening:

	GTI [W/m^2]	Θ [°]	T_{air} [°C]	V_{wind} [m/s]	V_{comp} [V]	V_{valv} [V]	Fr_{water} [kg/h]
A	922.56	20.29	9.45	0.77	4	4	342.04
B	962.46	22.87	14.09	0.87	4	4	367.69
C	806.84	26.55	4.75	1.42	4	4	295.76
D	812.46	32.16	13.41	1.26	4	4	338.36
E	1005.11	14.79	14.83	1.22	5	4	448.34
F	802.76	28.92	5.86	1.14	5	4	339.71
G	961.71	16.73	5.70	0.94	5	4	381.64
H	879.65	24.32	8.52	1.01	5	4	377.29
I	883.12	20.57	9.01	1.18	7.5	4	490.41
J	1036.10	19.66	14.74	0.71	7.5	4	578.22
K	878.07	22.02	6.03	1.15	7.5	4	489.06
L	750.64	31.90	9.01	0.40	7.5	8	127.76
M	942.55	20.50	14.17	1.26	7.5	8	101.80
N	1058.44	13.22	15.30	0.85	10	4	361.51

Table(5) PVT validation input data

This simulation is performed and the results are collected and compared to the measured data. The data collection performed at point “N” shown was performed to check the system’s operation when the compressor works at maximum speed . The results of the model, in terms of heat exchanged in both the evaporator and gas cooler, power consumption at the compressor, and electrical production of the PVT system are compared with experimental data. All these simulations were performed using Fortran, a programming language especially suited to numeric computation and scientific computing.

In the following graph all results of this comparison are reported:

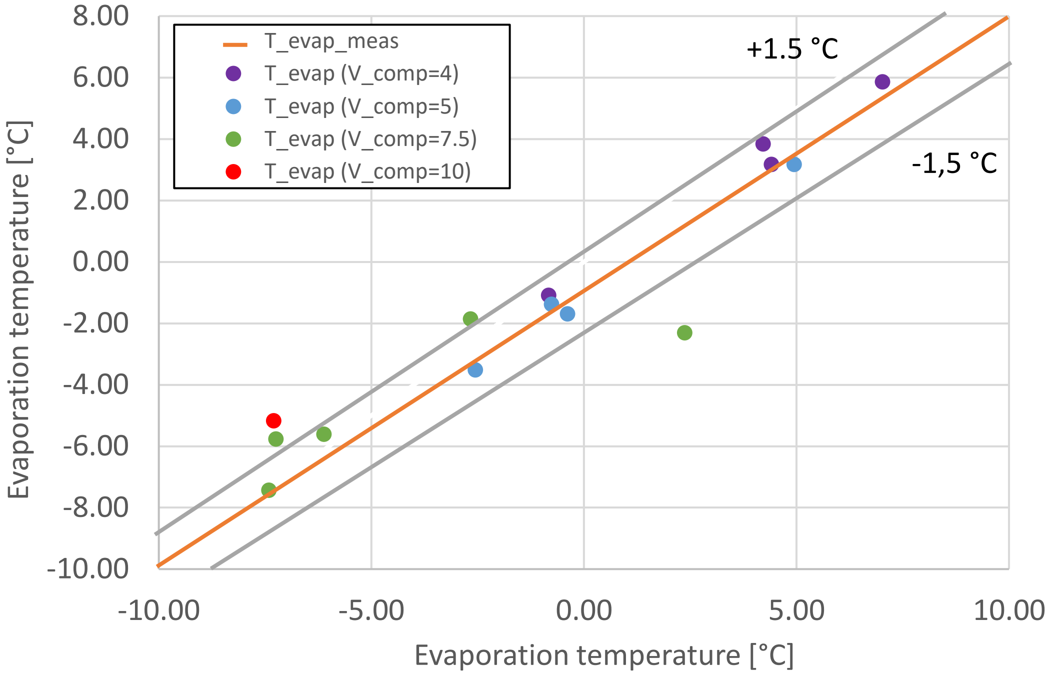

Figure(15): Evaporation temperature comparison, simulated vs. measured

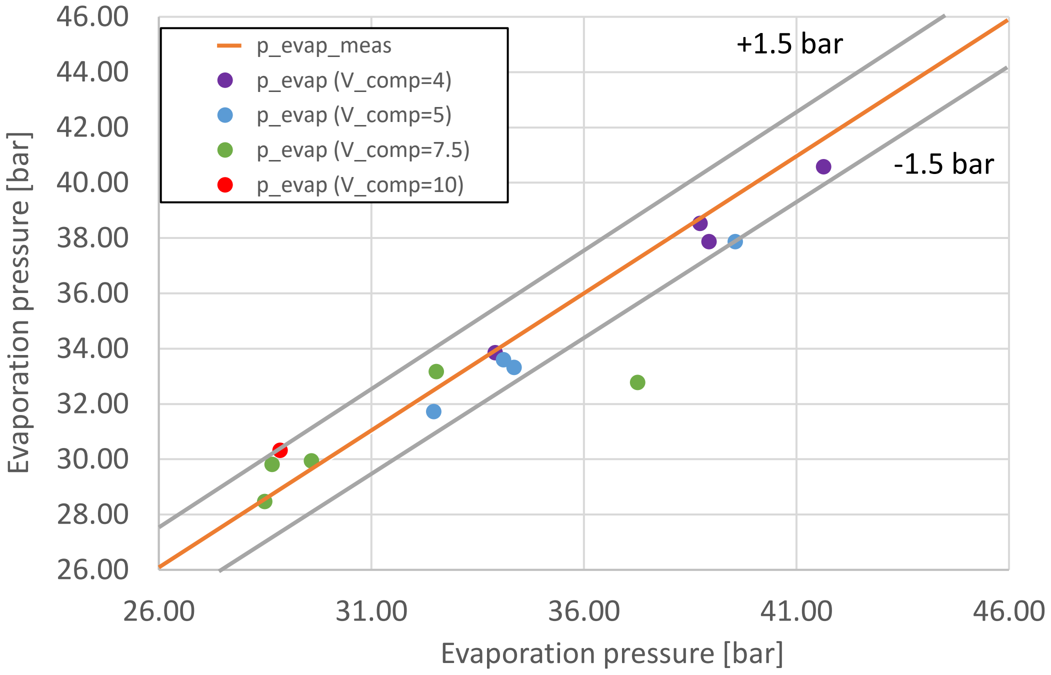

Figure(16): Evaporation pressure comparison, simulated vs. measured

Figure(15) and Figure(16) compare the simulated and measured values of evaporation temperature and pressure. An error band of 1.5°C and 1.5 bar is given as control. These results show that all simulations performed well, giving an error lower than the chosen one despite the simulations conducted with high pressure at the gas cooler (V_{valv}=8) and high compressor speed (V_{comp}≥7.5). Regarding the evaporation temperature the maximum error is reached at point "N" with V_{comp}=7,5 and V_{valv}=8. In this case the absolure error is equal to 4.67°C. Also for the evaporation pressure the maximum error is obtained in row "M" in the input table(5) with a value of 4.49 bar. This results is far from all the other measurement made for the system and we can neglect it from the discussion. This could be due to a bad measurement.

When the pump runs at its top speed, row "M", the errors obtained are: 2.12°C for the evaporation temperature and 1.47 bar for the evaporation pressure. These are the highest error obtained by the simulation when we don't consider the case seen in "M". From these two graphs it is noticeable that there is a correlation between higher pump speed and higher error.

In Figure(17), Figure(18), Figure(19), and Figure(20), the comparison between the measured and simulated values of heat of vaporization, the heat delivered at the gas cooler, the compressor's power consumption, and the electrical power generated by the PVT system is reported. For these data an error band of ∓10% is given as control.

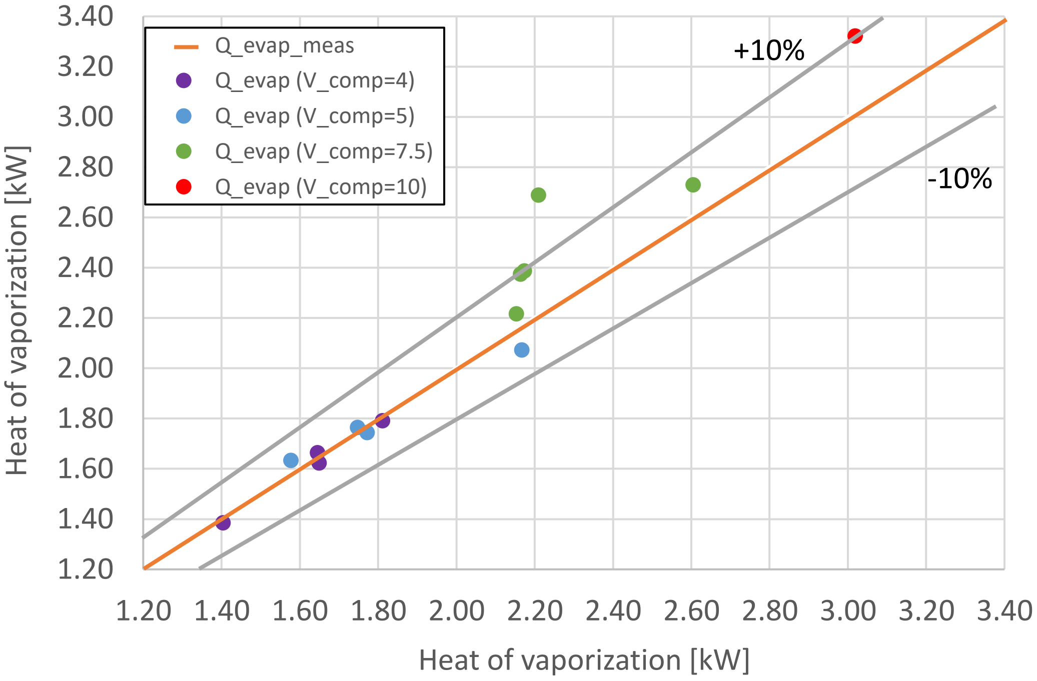

Figure(17): Heat of vaporization comparison, simulated vs. measured

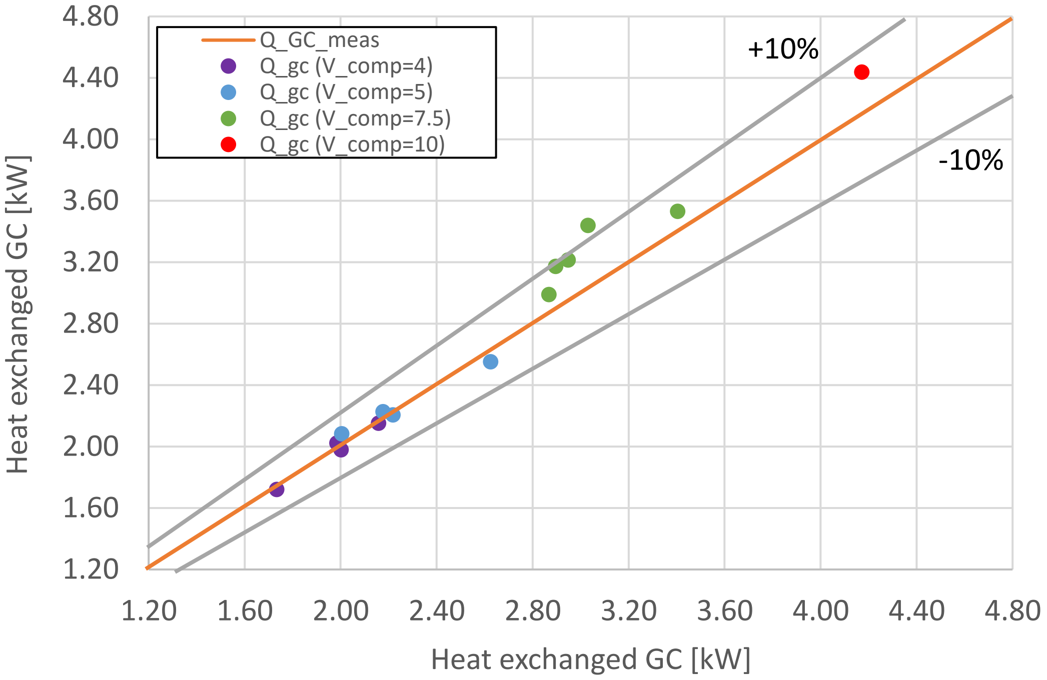

Figure(18): Heat delivered at the gas cooler comparison, simulated vs. measured

Also the heat exchanged on both the evaporator and the gas cooler are well simulate as the error is always between the ∓10% error bands despite of case "M" as seen in Figure(15) and Figure(16). Also in this case the maximum error is reached in case "M" with a value of 22% for the heat of vaporization and 14% for the heat exchanged at the gas cooler. The relative error ξ for the heat of vaporization: $\xi<2\%$ when $V_{comp}=4$; $2\%<\xi<4\%$ when $V_{comp}=5$, $4\%<\xi<10\%$ when $V_{comp}=7.5$, $\xi=10\%$ when $V_{comp}=10$. A similar trend in followed for the heat exchanged at the gas cooler.

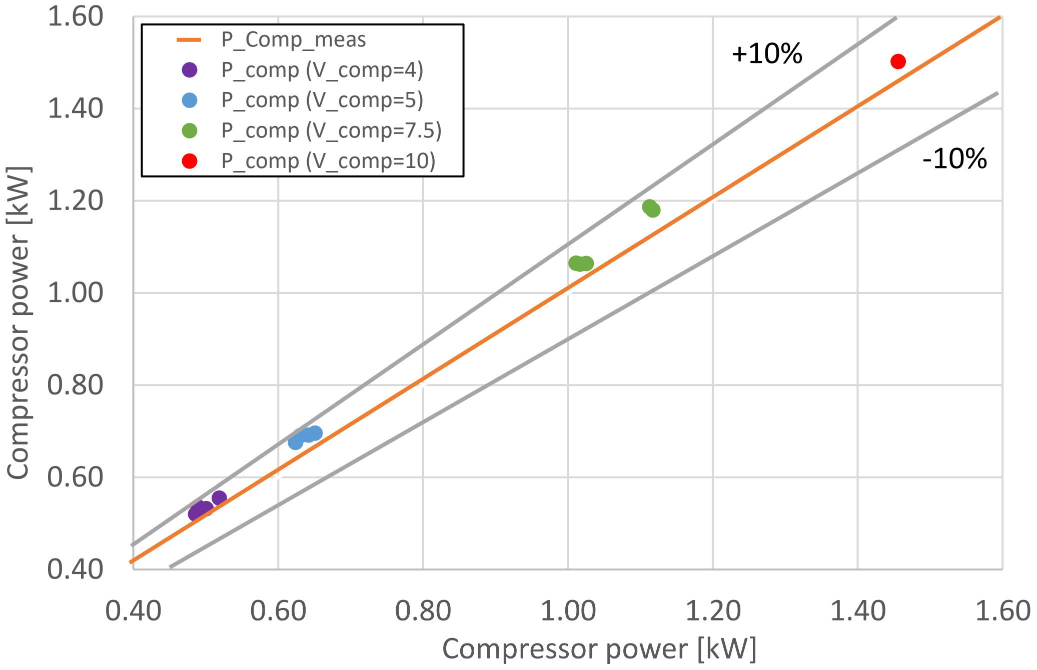

Figure(19) Compressor power consumption comparison, simulated vs. measured

The power consumption at the compressor is calculated with three-variable polynomial of three degree equation depending by the evaporation temperature, the pressure at the gas-cooler and the compressor speed. This equation is presented by Zanetti et al. in [34]. In this case the there is not a correlation between the error and the pump speed as the simulation overestimate the power consumption by 5% to 9%.

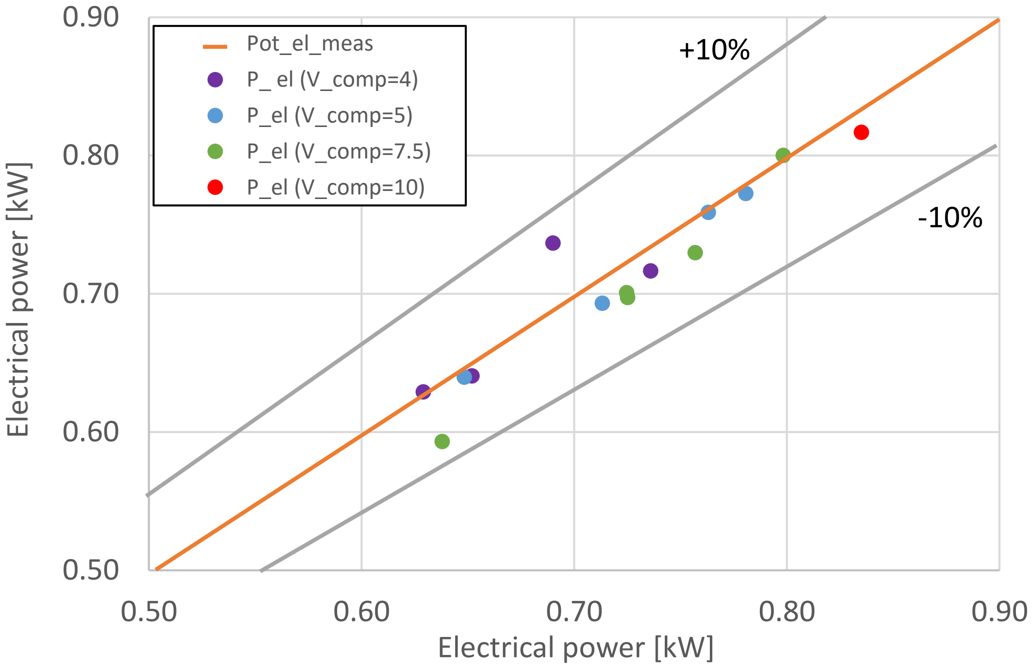

Figure(20): Electrical power production, simulated vs. measured

The electrical power production is obtained as the energy flux converted into electrical power by the PV system via eq(13). As seen in 3.2.2 this equation depends on the values of the coefficients η_{PV} and T_{ref-PV}, which can be found in the PV or PVT panel datasheet, and the value of the efficiency deviation parameter b_{PV} and the incident irradiance G·A. This calculation does not depend on the pressure level or the pump speed indeed in Figure(20) there is no correlation between the measurement and their errors. Also in this case the simulation results follow the measurement giving a maximum error of 7%.

In appendix A all the results are reported.

5.2.3 Finned coil simulation

Figure (21) and (22) depict the model's outcomes for the heat pump's operation with the finned coil heat exchanger on the same test day illustrated in Figures 4 and 5. Measures are represented by dashed lines, while continuous lines represent the simulation results. The shaded areas in the figures indicate the periods when the heat pump is in operation. Specifically, Figure(21) showcases the water temperature at the gas-cooler outlet and the water flow rate. The temperature trends of both measured and simulated data align with a maximum deviation of approximately 3°C. Figure 12 highlights that the gas-cooler outlet temperature is heavily dependent on the water mass flow rate in circulation within the system.

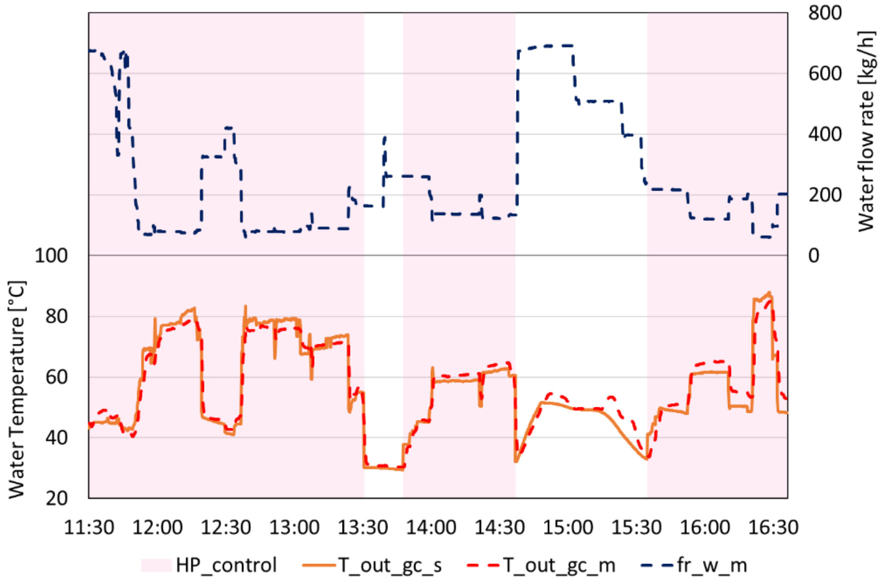

Figure(21) Water temperature at the gas-cooler outlet, simulated (s) and measured (m) data comparison and measured water mass flow rate (fr). The finned coil is used as the evaporator. [34]

Figure(22) illustrates the water temperature readings obtained from both measurements and simulations at the TANK2 level. Specifically, the temperature at the gas-cooler outlet (TANK2 inlet) is compared with the temperature at the top and bottom portions of the thermal storage. As a result of the thermal stratification within the tank, there is a time delay in the water temperature peaks between the entering temperature and the outlet temperature of the storage. The TRNSYS model's results agree with the measured data, with a maximum temperature deviation of about 5°C. This deviation is attributed to the model's higher thermal inertia and quicker reaction to the flow rate variation in comparison to the experimental data, resulting in a lengthier delay of the thermal response. Moreover, temperature discrepancies at the TANK2 outlet have an impact on the temperature at the outlet of other plant components. The trend in the temperature at the outlet of the plate heat exchanger and the water temperature leaving the mixing valve is similar, slightly ahead of the measured data.

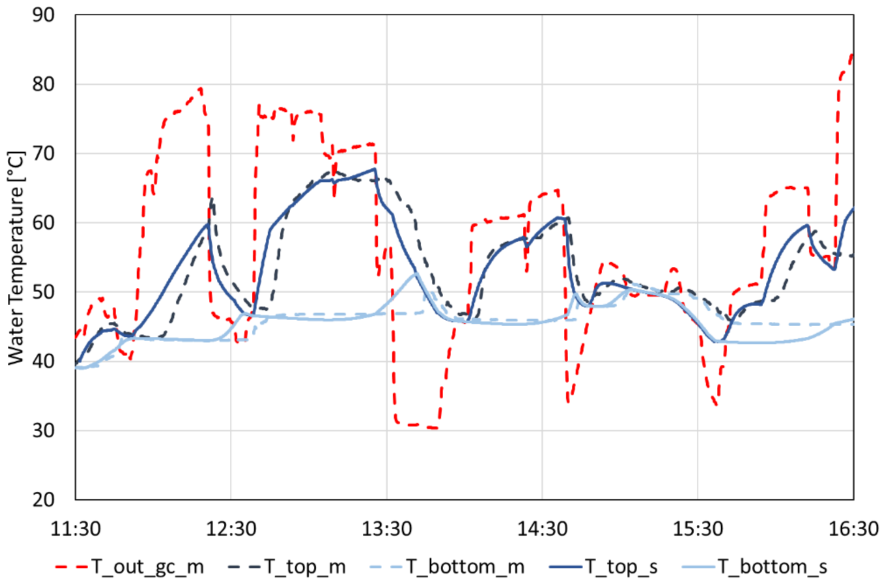

Figure(22) Simulated (s) and measured (m) data comparison of water temperature at the TANK2 bottom and top nodes and water temperature at the gas-cooler outlet. The finned coil is used as the evaporator. [34]

5.2.4 PVT simulation

The heat pump analysis was conducted with the PVT acting as the evaporator. The figures depict the simulated results with continuous lines and the measured data with dashed lines. The shaded regions in the figures indicate the periods when the heat pump is operational. Dynamic simulations were carried out using the calibrated model of the hydronic circuit. Figure(23) presents the water temperature at the gas-cooler outlet and the water flow rate when the heat pump is connected to the PVT panels. The simulated temperature trends and the measured temperature are in excellent agreement. However, the maximum deviation is observed when the heat pump is switched on, and there are sudden changes in the water flow rate. In such operational conditions, the model fails to accurately simulate the unit's inertia, which does not immediately respond to the water flow rate variation or reach full power instantly after activation in practical applications.

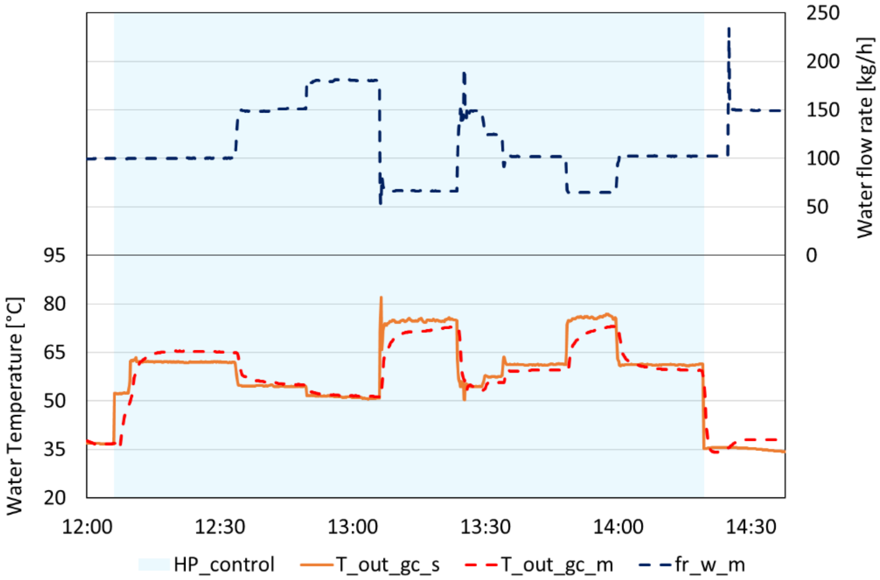

Figure(23). Water temperature at the gas-cooler outlet, simulated (s) and measured (m) data comparison and measured water mass flow rate (fr). PVT panels are used as the evaporator. [34]

In Figure(24), the simulated and measured thermal power generated by the heat pump and exchanged in the gas-cooler, along with the overall electrical power absorbed by the heat pump, are displayed. The measured and simulated data exhibit good agreement, with a relative error of less than 10% in both values. The coefficient of performance (COP) can be determined by dividing the thermal energy generated by the heat pump by the electrical energy absorbed. The experimental tests yielded a COP of 2.63 during the ON period, and a COP of 2.43 when the standby phase (when only the heat pump's electronics are active) is also taken into account. The simulated COP during the ON period is 2.58, which is only slightly less than 2% lower than the experimental COP value.

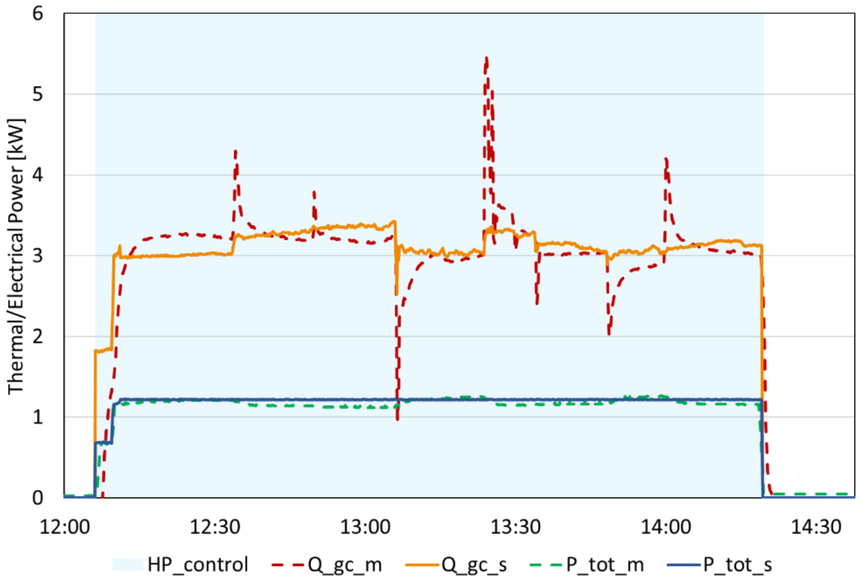

Figure(24) Heating capacity in the gas-cooler and electrical power overall absorbed by the heat pump, simulated (s) and measured (m) data comparison. PVT panels are used as the evaporator. [34]

Figure(25) displays the measured and simulated values of photovoltaic power production, along with the Global Tilted Irradiance. The agreement between the simulated and measured data is satisfactory in both cases, i.e., when the heat pump is ON and the evaporating CO2 cools the PVT panels, and when the heat pump is OFF, and there is no cooling of the PV cells. However, the PVT model does not account for the thermal capacitance of the solar collectors, and it is incapable of simulating the panels' thermal inertia. This deficiency is evident in Figure 16, where at around 14:20, the heat pump is deactivated, and the simulated electrical power production considerably drops due to the PV cells' instantaneous temperature increase, which impairs their electrical efficiency.

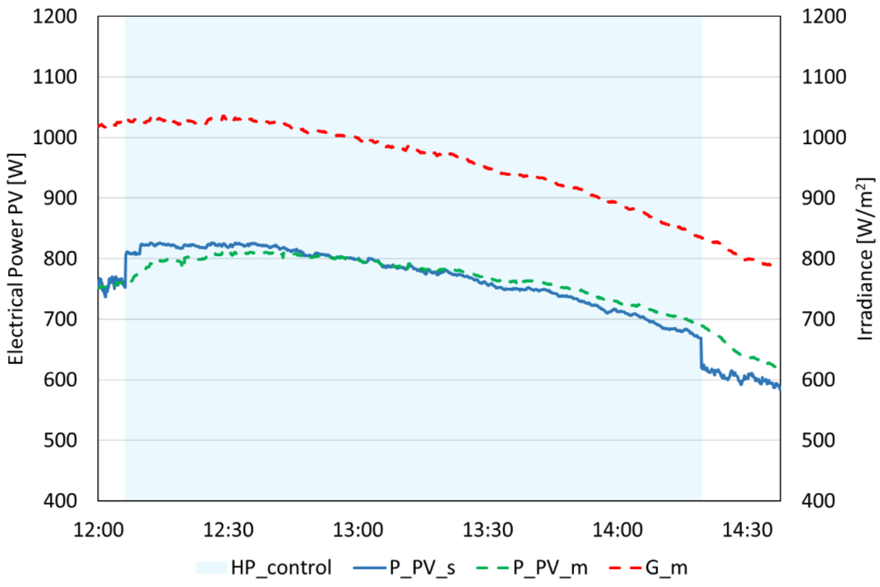

Figure(25) Global Tilted Irradiance (G) and photovoltaic power production (P_{PV}), simulated (s) and measured (m) data comparison. PVT panels are used as the evaporator. [34]

The prototype underwent experimental testing under dynamic conditions in both air and solar modes with real solar irradiance and air temperature. During testing, the refrigerant released heat to water in the gas-cooler, which was then stored in a water tank and withdrawn by a plate heat exchanger when the user requested a thermal load. The maximum thermal load provided to the user was 8 kW, and the maximum heating capacity at the gas-cooler was 5 kW.

During experimental testing in solar-mode, the cooling effect of the refrigerant evaporating in the PVT collectors led to an 8% increase in photovoltaic power production when the heat pump was switched on.

The model evaluated temperature values at the inlet and outlet of the hydronic system and the gas-cooler heating capacity, electrical power absorbed by the heat pump, and electrical power produced by the PVT collectors. The simulated COP of the heat pump (when switched on) was found to be 2.58, less than 2% lower than the value estimated through experimental testing. The validated model can be a valuable tool for seasonal simulations and developing a control strategy to optimize the benefits of a dual-source system.

6. Seasonal simulation

The new validated TRNSYS model is used to simulate the operation during the heating season in Venice, from the 1st of January to the 15th of April. The TRY data from EnergyPlus were used. Two tests have been performed:

1. In air mode, the heat pump uses the finned coil evaporator
2. In solar mode, the heat pump uses the PVT as evaporator

This simulation has been carried out in TRNSYS Simulation Studio these tests have been conducted to verify the dynamic behavior of the model simulating the production of domestic hot water. The system modelled in the TRNSYS environment is shown in Figure(26).

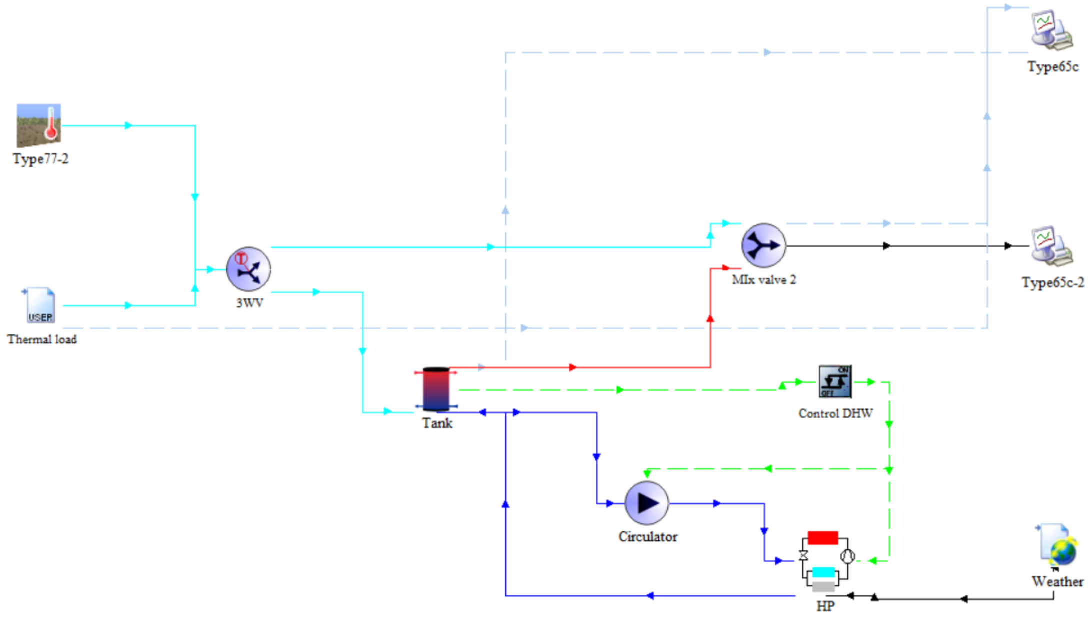
Type65c
Type77-2
3WV
MIx valve 2
Type65c-2
USER
Thermal load
Tank
Control DHW
Circulator
HP
Weather

Figure(26) Scheme of the system modelled in Simulation Studio (TRNSYS)

Module name	**Module icon**	**Module introduction**
Inlet water – Type 77-2	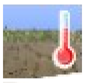	Type used to simulate the aqueduct water's temperature
Weather – Type 15-3		Type used to read the weather input for Venice
HP - Type 211	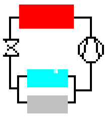	The mathematical model of the heat pump.
Module name	**Module icon**	**Module introduction**
Tank - Type 534	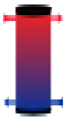	Heat exchanger water tank
Mixing valve – Type 11h		Valve used to mix water coming from the hot tank and the aqueduct
3WV – Type 11-b	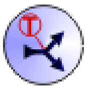	3 way valve : Part of the water coming from the aqueduct flows to the tank, the rest to the mixing valve
Circulator – Type 3d	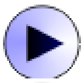	Pump model, controls the flow rate to the heat pump
Printer – Type 25c		Collects and print results
Data reader – Type 9e		DHW demand profile

Table(6) Type used in Simulation Studio

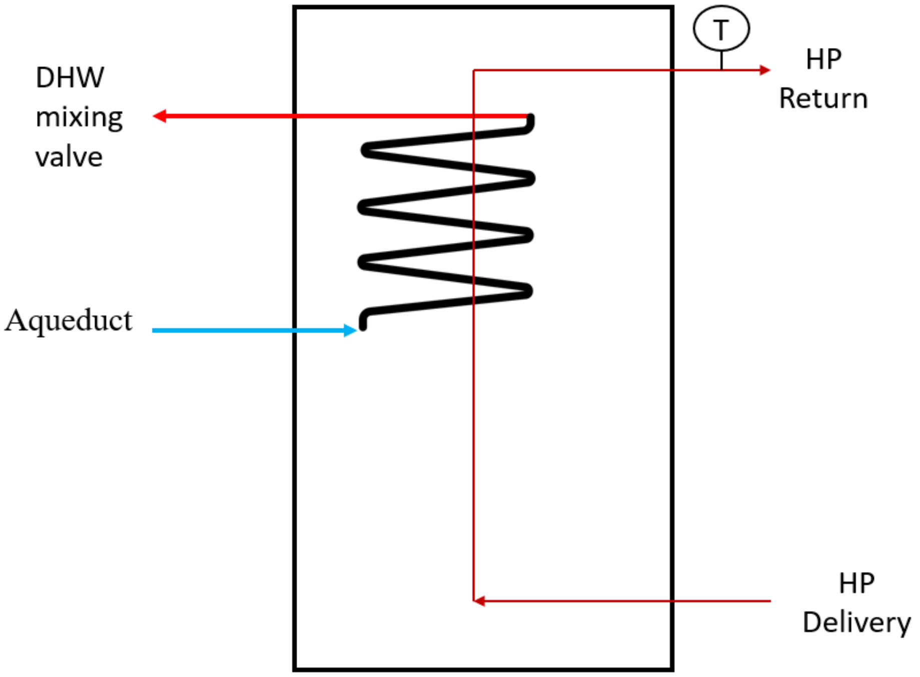

Figure(27) Water tank with internal heat exchanger

When the DHW request is turned on, water coming from the aqueducts flows to the three-way valve (3WV): here part of the water is sent to the tank, the other part flows directly to the mixing valve. A simplified scheme of the heat exchanger water tank is presented in Figure(27). The tank is divided, in the model, into 8 isothermal nodes: the upper node is node 1 and the bottom node is node 8. The municipality water enters the immersed heat exchanger which occupies nodes 1 to 5, and after being heated in the thermal storage, enters the mixing valve from the upper node of the DHW tank. The hot water produced from the heat pump's gas cooler enters the DHW tank from node 8, releases heat to the municipality water and returns to the heat pump's source side from the upper node.

The setpoint temperature of the tank is equal to 50°C. When the water outlet temperature from the tank goes below the set point lower dead band(50°C-3°C=47°C), the circulator (Circulator) and the heat pump are switched on, the pump start to run a flow rate equal to 700 l/h in order to heat up the water inside the coil. In Figure(26) this closed water loop is presented in blue. The DHW stored in the tank is heated up by this internal heat exchanger and the system is turned off when the upper dead band (50°C+1°C=51°C) is reached. The heated DHW is then sent to the mixing valve where it is mixed with the cold water from the aqueduct. The resulting water temperature is delivered to the user.

In figure(28) the air temperature and global irradiance on tilted surface profile during the seasonal simulation are presented. The requested DHW flow rate shown in Figure(29) is derived statistically from DHW calc, based on an average daily withdrawal by a user of 200L/day.

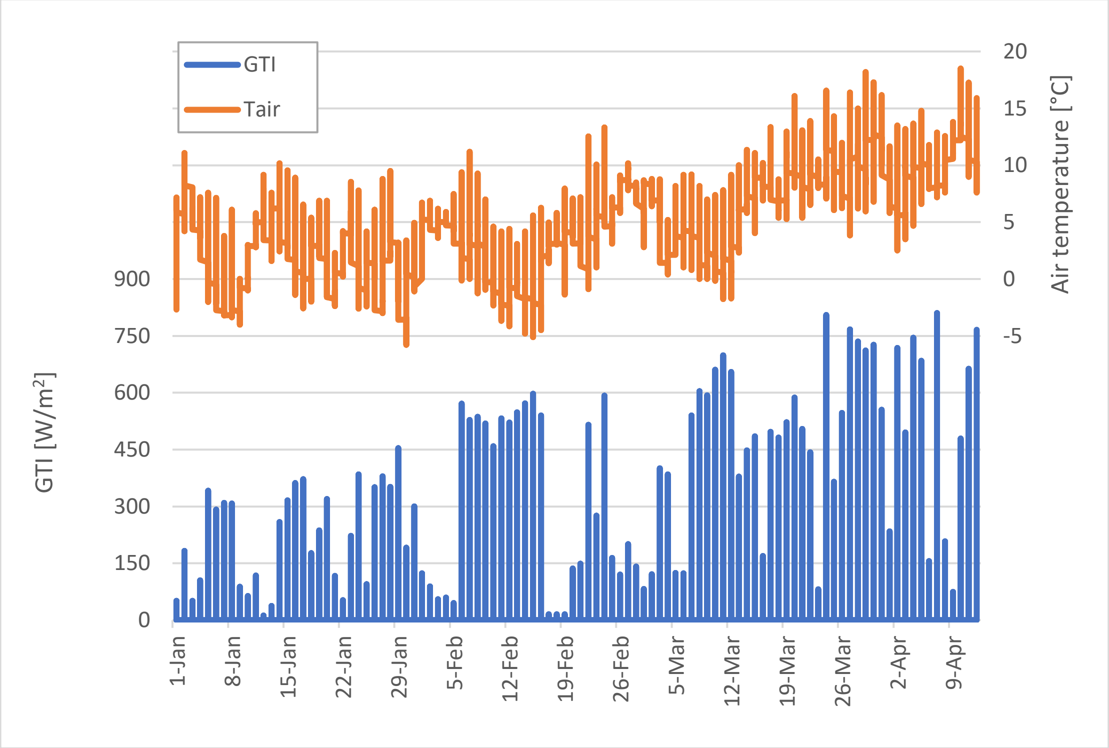

Figure(28) GTI and air temperature profile

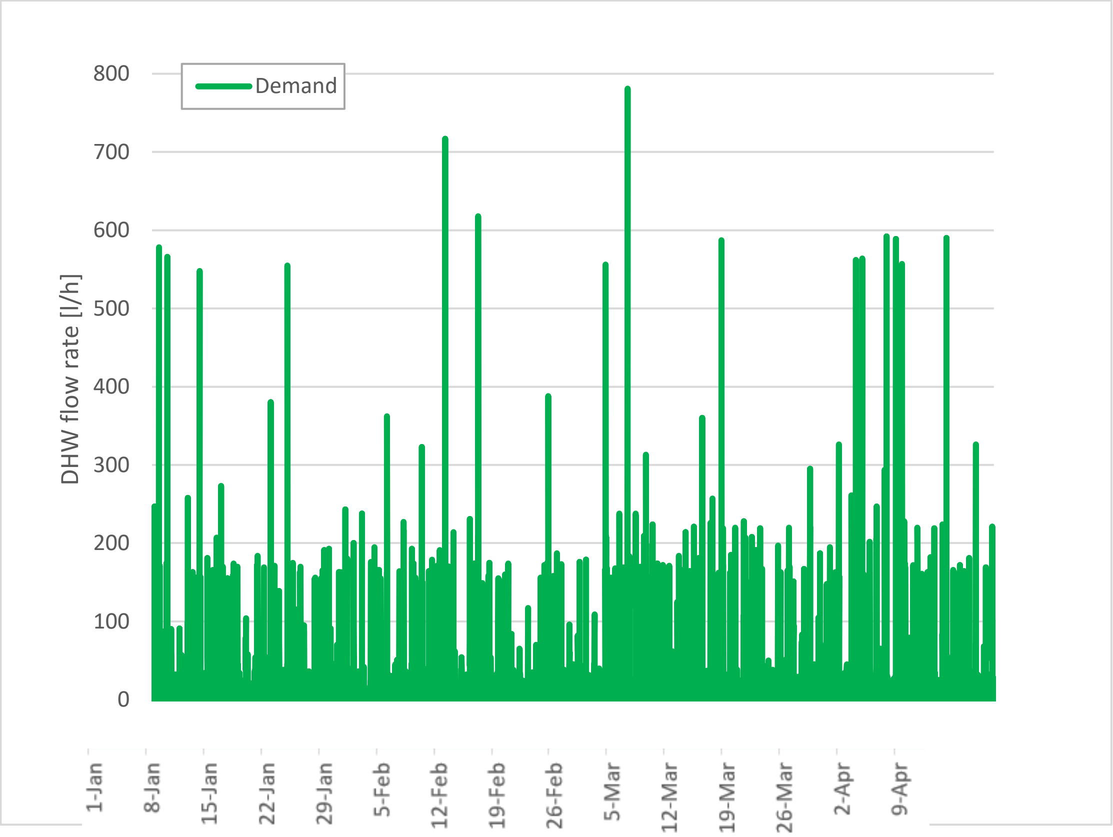

Figure(29) User flow rate demand

6.1 Results of seasonal simulation

The goal of these simulations is to deliver water to the user always at a temperature higher than 40°C by mixing the cold water from the aqueduct with the hot water preheated in the internal heat exchanger in the tank. Both simulations reached the desired results, the delivery temperature is almost reached for every request as can be seen in figure(30).

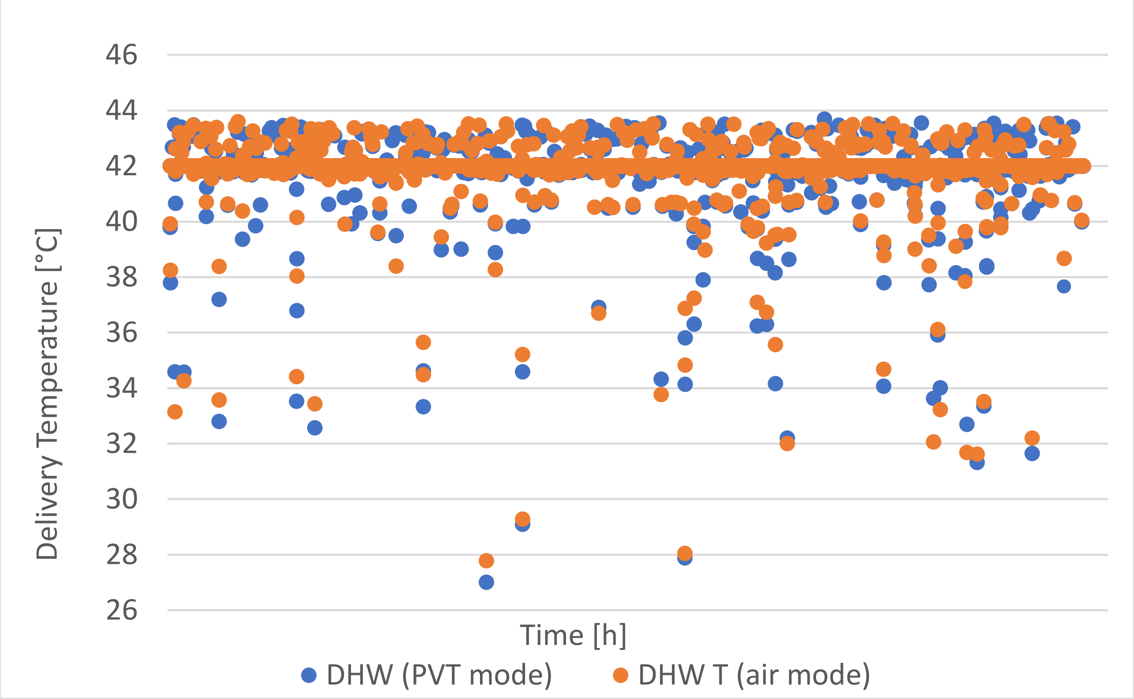

Figure(30): Delivery temperature in the heating season (1st of January - 15th of April)

Figure(27) and figure(28) show, as an example, the temperature profile of the water inside the DHW tank and the supply temperature in both PVT and air modes, during three days (72 hours) in April. The delivery temperatures is quite the same in both mode in the evaluated heating season, as it is noticeable from figure(31) and figure(32).

The heat pump is able to heat up the water that flows outside from the tank. In these two figures we can see that "Tank T outlet" is kept between the two dead bands and the heat pumps turns on every time the temperature goes below the lower dead band. The delivery temperature setpoint is always reached except when the requested DHW flow rate is higher than 5 l/min=300l/h.

It is important to limit the ON/OFF cycles in order to extend the life of the heat pump. The graphs show a higher number of switching on of the heat pump in air mode, compared to the PVT mode.

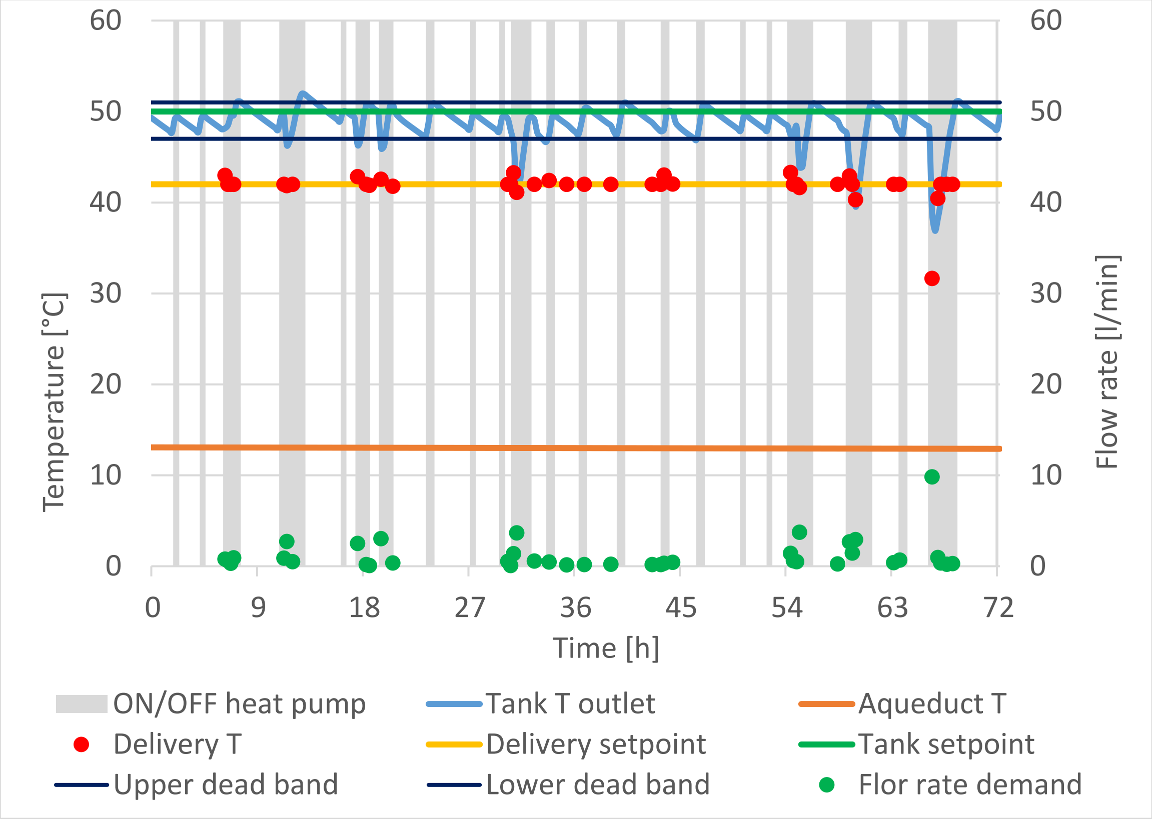

Figure(31): PVT mode, Tank temperature profile and flow rate request

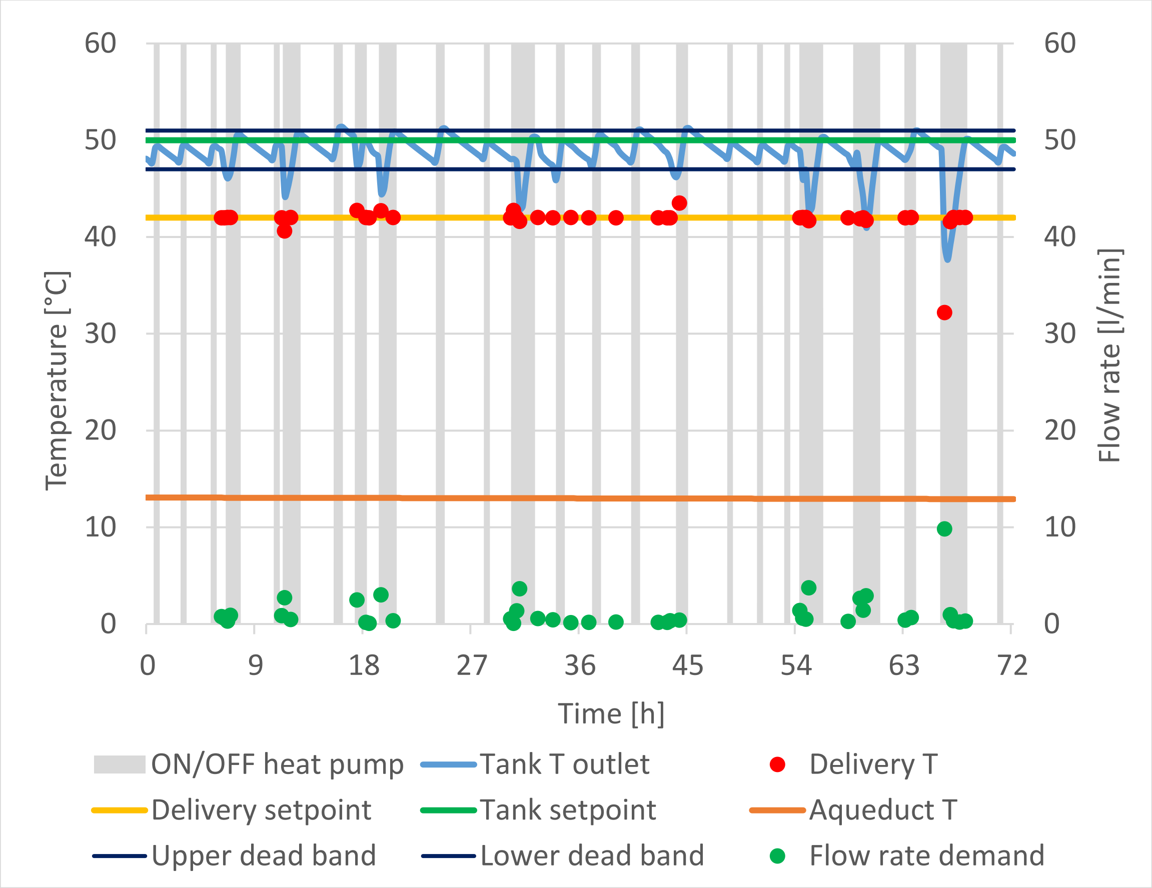

Figure(31): Air mode, Tank temperature profile and flow rate request

Another important parameter to check is the electrical power generated by the PVT module during different moment of the year. In figure(32) and Figure(33) the heat pump's power consumption and the electrical power generated by the PVT module are reported respectively in the first week of January and April:

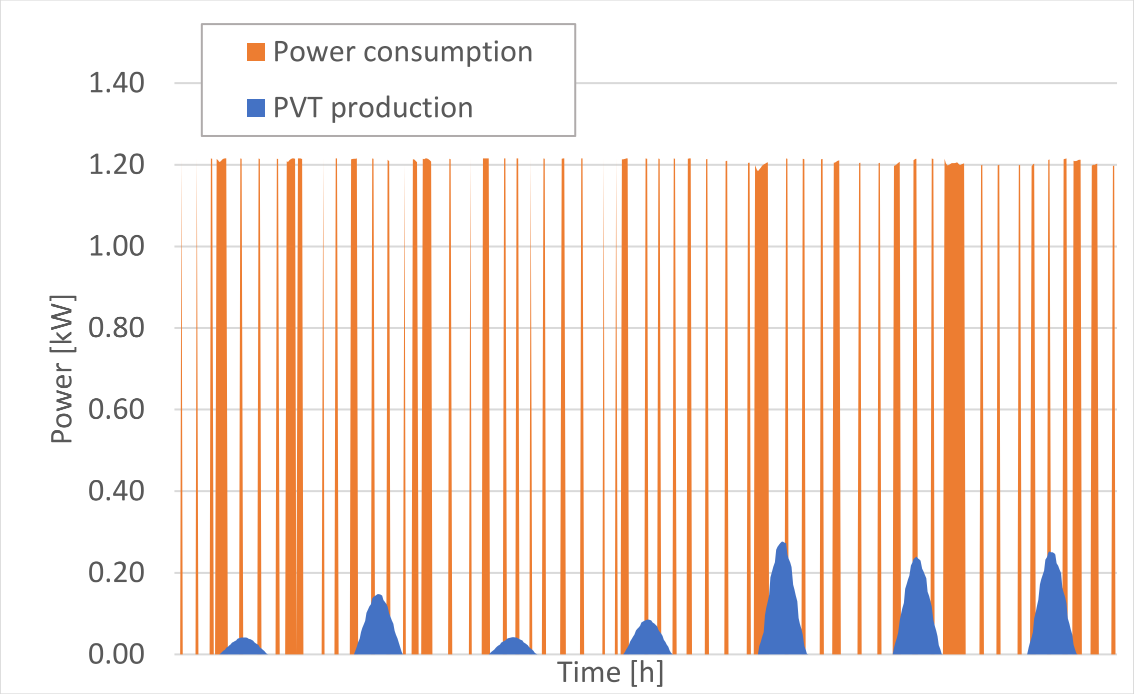

Figure(32):Power consumption and PVT production (1st January – 7th January)

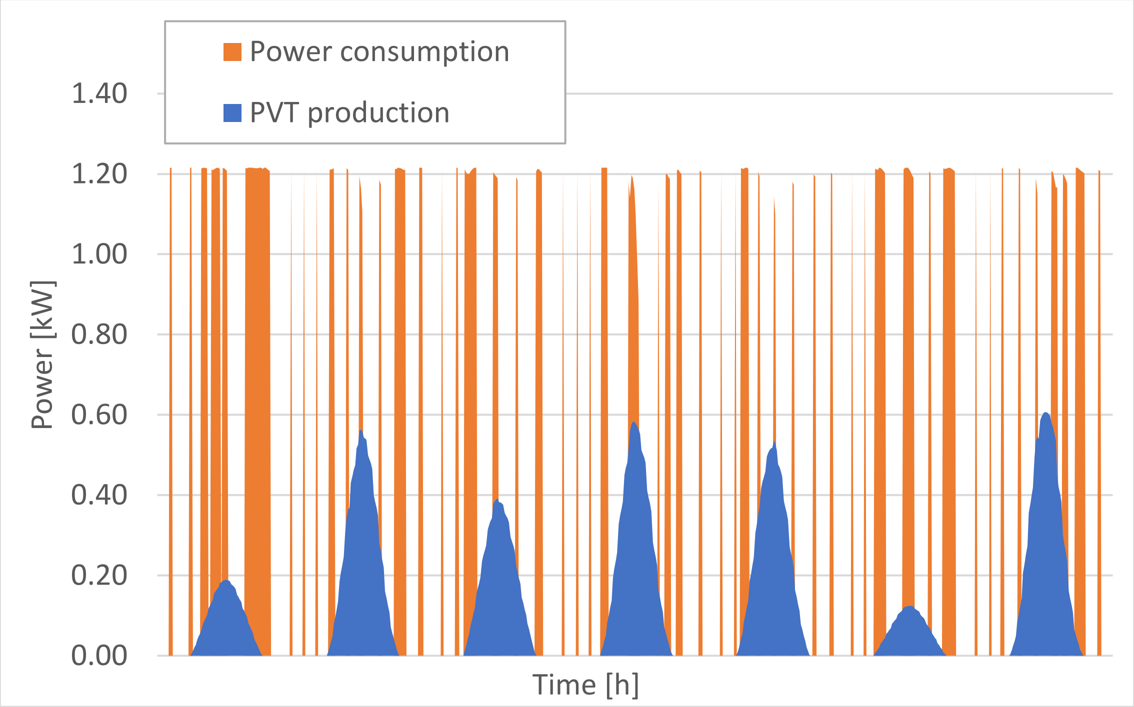

Figure(33):Power consumption and PVT production (1st April – 7th April)

The PVT electrical power production is higher in April, when the GTI is higher. In the seasonal simulation the heat pump general power consumption P_{gen} is calculated as:

$$P_{gen}=P_{comp}+P_{vent}+P_{cont} \qquad (21)$$

It's important to remember that P_{vent}=0 when the PVT is used, indeed only the finned coil heat exchanger uses the fan. P_{cont} accounts for the power absorption due to the heat pump's electronic devices. P_{cont} is a constant value equal to 0.0288 kW.

The resulting consumed power during the considered heating season, in kWh, is P_{gen}=740.75 kWh and the total electrical power generated by the PVT module is P_{el}=167.96 kWh. Its interesting to calculate the electrical power generated while the heat pump is turned ON, in this case P_{el}=46.74 kWh.

An assessment must be made on the simultaneity of production and consumption, unused electrical power can be stored in a battery or sent to the network if the system is connected to the grid. In the best possible scenario all the produced power is instantaneously consumed by the heat pump. Non-contemporaneity between production and consumption is, however, one of the biggest issues of non-programmable renewable sources.

To evaluate this problem we can calculate two different parameter:

1. Coverage ratio(1): in case of the presence of a battery used to store the electrical power produced when the heat pump is turned off. This parameter shows how much energy consumption is covered by the PVT in percentage. It is calculated as:

$$C_{ratio,1}= \frac{P_{el}}{P_{gen}} \tag{22}$$

   In this case $C_{ratio,1}$ = 22.67%

2. Coverage ratio(2): this parameter similarly to the one seen in equation (22) evaluates the ratio of the electrical power produced by the PVT can be used directly by the heat pump when there is not any battery. In this case we have to filter all the data in order to use the power produced by the PVT only when the heat pump is ON.

$$C_{ratio,2}= \frac{P_{el,HPon}}{P_{gen}} . \tag{23}$$

   In this case $C_{ratio,2}$ = 6.31%

It is clear that the presence of a battery improves the overall performance of the machine as the coverage increases noticeably.

To evaluate the seasonal performance of the system it is important to calculate the COP and the SCOP for both air mode and PVT mode: in Figure(34) and Figure(35) the COP trends for two days in January and two days in April are reported. The solar irradiance is quite the same in these two tests and the main difference is the air temperature with a mean values of 6°C and 14°C respectively.

A third results is shown in figure(36) for two days in March with a much higher irradiance.

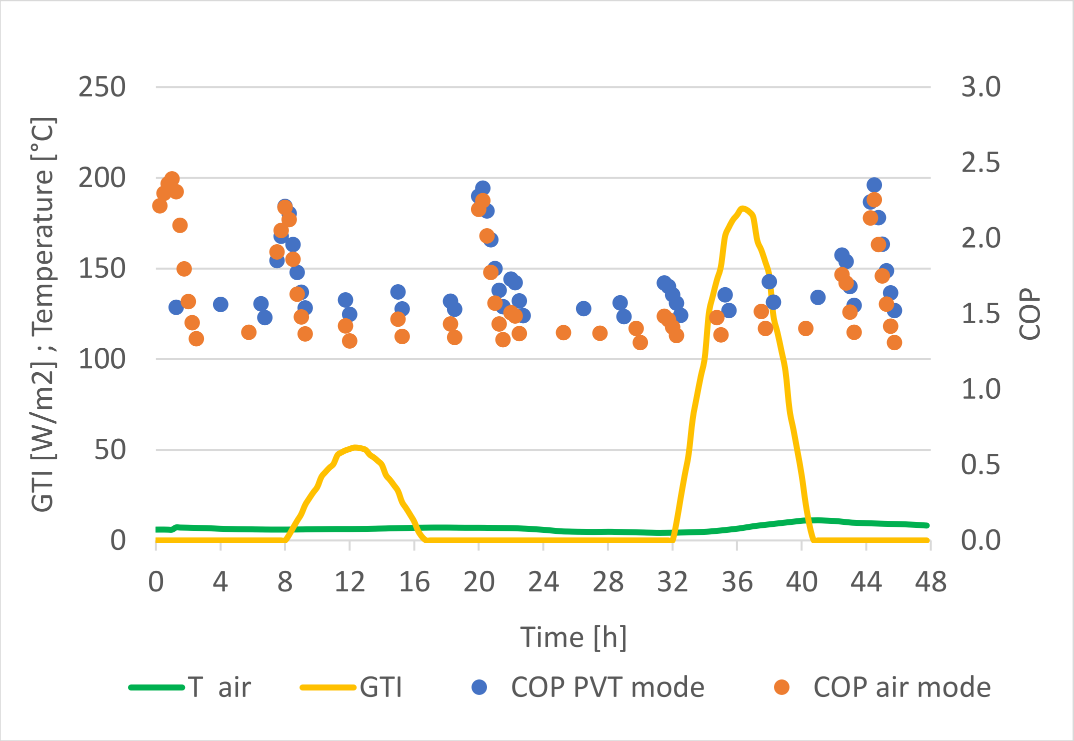

Figure(31): COP trend, January, lower radiation

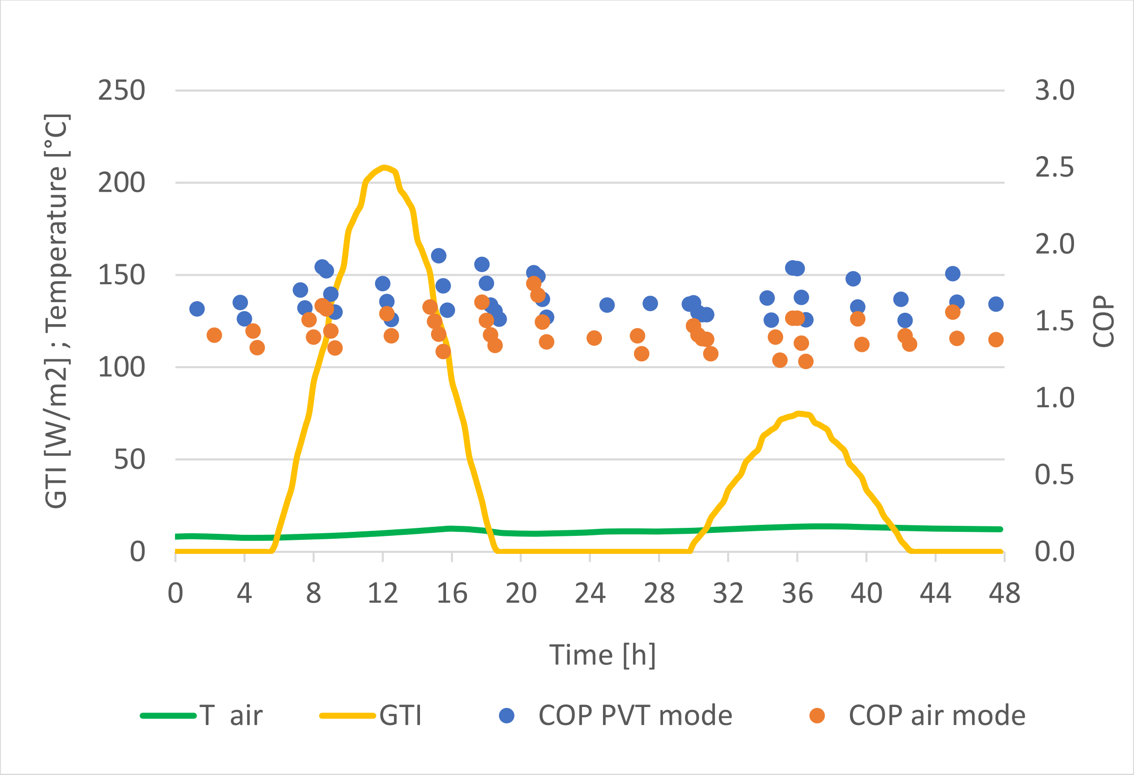

Figure(32): COP trend, April, lower radiation

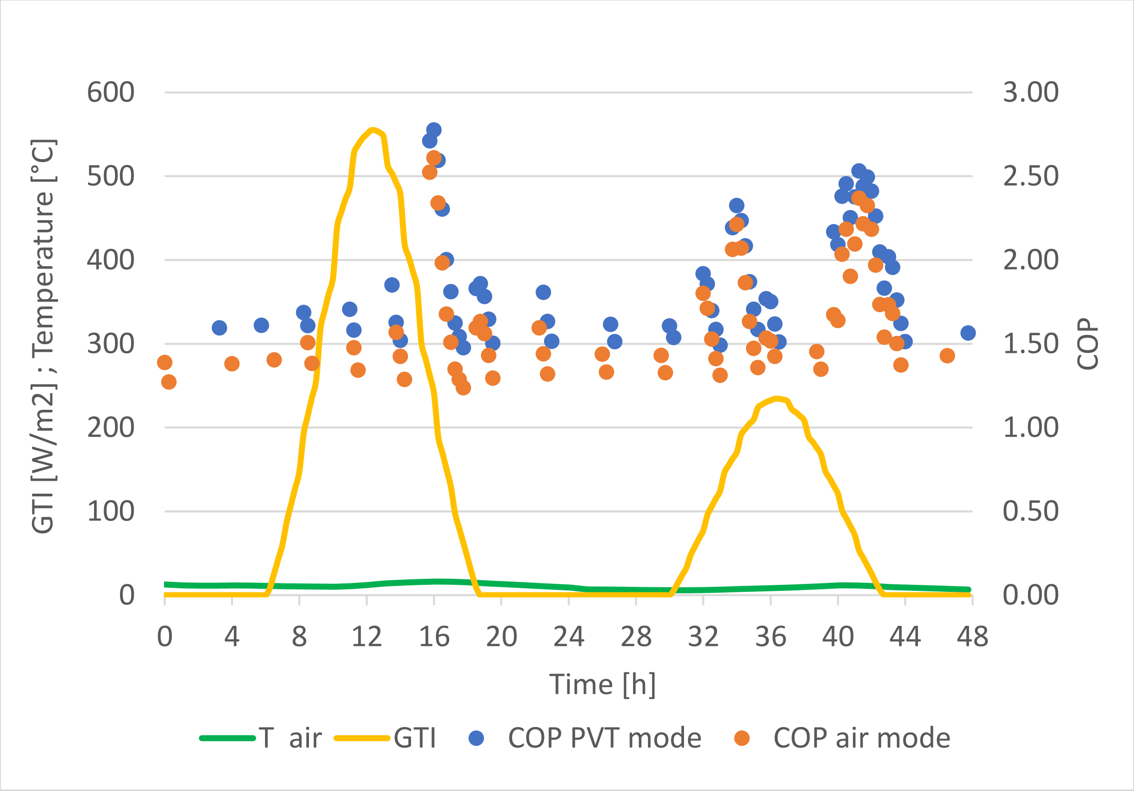

Figure(33): COP trend, April, higher radiation

In Figure(31) and Figure(32) can be seen how the values of COP in these representative time span are nearly equal, the PVT mode gives a slightly higher values when the outside air temperature is higher (in April). The COP of the cycle isn't affected to much by solar radiation but it has to be reminded that in the PVT mode the electrical power production increases the overall performance of the machine. In this case this prototype is equipped with only three panels connected in series, this lead to an underestimated solar field for the system. In Figure(33) it is shown how an increasing solar radiation is correlated to an increase of COP. Here the gap between the COP values obtained in air mode and in PVT mode is higher this lead to interesting results in the operation when the irradiance is high and the external air temperature is low. During the seasonal simulation the maximum COP is reached when GTI is at its maximum value (COP=2,78 in PVT mode and GTI=780 W/m^2).

The mean COP value obtained by this simulation is lower than the one obtained by the transient simulation seen before. This could be due to system's configuration and the higher thermal load demanded by the user. In this simulation there is also a much higher water flow rate that exchanges heat with the refrigerant at the gas cooler.

Considering the seasonal coefficient of performance (SCOP) in PVT mode it is obtained a value of $SCOP_{PVT}$=1.63 and in ait mode it is equal to $SCOP_{air}$=1.47. Important to remember that in air mode there is also the contribution of the fan to the absorbed power.

7. Conclusion

This work presents the analysis of a multi-source system consisting of an air source heat pump coupled to a PVT system and a finned coil.

The purpose of the work was to analyze the functioning of the heat pump prototype within a system that simulates the withdrawal of a heat load by a user, within the TRNSYS environment.

The heat pump model coupled with the PVT collectors was validated using the experimental data. simulations were firstly performed with some punctual inputs, giving good results as the errors are below the set error band. The evaporation temperature and pressure error were always below ±1,5 °C and ±1,5 bar with an increasing error as the compressor speed increased. Also the percentage error on the Heat exchanged at the gas cooler and the evaporator were below ±10% and followed the same trend. The power produced by the PVT module and the power consumption gave low error values with no dependence on the compressor speed or valve opening. Here the two equation used well simulate the real functioning of the machine with no compromises.

In addition, the dynamic behaviour of the experimental plant was considered and the results of the model, developed using TRNSYS, were compared to the experimental data. During testing, the refrigerant released heat to water in the gas-cooler, which was then stored in a water tank and withdrawn by a plate heat exchanger when the user requested a thermal load. The maximum thermal load provided to the user was 8 kW, and the maximum heating capacity at the gas-cooler was 5 kW.

During experimental tests in solar-mode, the cooling effect of the refrigerant evaporating in the PVT collectors led to an 8% increase in photovoltaic power production when the heat pump was switched on.

The model evaluated temperature values at the inlet and outlet of the hydronic system and the gas-cooler heating capacity, electrical power absorbed by the heat pump, and electrical power produced by the PVT collectors. The simulated COP of the heat pump (when switched on) was found to be 2.58, less than 2% lower than the value estimated through experimental testing.

Finally the validated model is used as a tool for seasonal simulations. The dual-source heat pump was assumed to work provide domestic hot water to a residential unit, located in Venice. The heat pump model was used to simulate the operation of the system during the heating season in (From the 1^{st} of January to the 15^{th} of April). In this case the system was able to cover the DHW request at the set delivery temperature,42°C, all the season. The power production of the PVT module were calculated in order to be compared with the general power consumption of the heat pump. Considering the overall production, in case a system with the presence of a battery (electrical power storage) it was valued that the PVT was able to cover 22.67% of the power needs of the system

Considering only the simultaneous functioning of the heat pump and the PVT generator only 6.37% of the power requirement was covered,

Lastly, a comparison between the SCOP of both functioning mode was made: in this simulation the PVT performed better than the air source mode, giving an higher $SCOP_{PVT}$=1,63 than the $SCOP_{Air}$=1,47. This result could be due to the power consumption of the fan and due to a better exploitation of the solar resource.

In a future study a choice strategy will be defined in order to understand when it is preferable to use a source instead of the other making other comparison between different simulations even in different climatic zones

References

[1] “What is the Kyoto Protocol? | UNFCCC.” https://unfccc.int/kyoto_protocol (accessed Mar. 20, 2023).

[2] “The Paris Agreement | UNFCCC.” https://unfccc.int/process-and-meetings/the-paris-agreement? (accessed Mar. 20, 2023).

[3] “Renewable energy directive.” https://energy.ec.europa.eu/topics/renewable-energy/renewable-energy-directive-targets-and-rules/renewable-energy-directive_en (accessed Mar. 20, 2023).

[4] “THE 17 GOALS | Sustainable Development.” https://sdgs.un.org/goals (accessed Mar. 20, 2023).

[5] “Climate Change Performance Index (CCPI).” https://ccpi.org/ (accessed Mar. 20, 2023).

[6] “An EU Strategy on Heating and Cooling 2016”.

[7] “Heating – Analysis - IEA.” https://www.iea.org/reports/heating (accessed Mar. 20, 2023).

[8] “Renewables steadily increasing in heating and cooling - Products Eurostat News - Eurostat.” https://ec.europa.eu/eurostat/en/web/products-eurostat-news/-/edn-20220211-1 (accessed Mar. 20, 2023).

[9] “Heating and cooling from renewables gradually increasing - Products Eurostat News - Eurostat.” https://ec.europa.eu/eurostat/en/web/products-eurostat-news/w/ddn-20230203-1 (accessed Mar. 20, 2023).

[10] “How a heat pump works – The Future of Heat Pumps – Analysis - IEA.” https://www.iea.org/reports/the-future-of-heat-pumps/how-a-heat-pump-works (accessed Mar. 20, 2023).

[11] “About heat pumps – European Heat Pump Association.” https://www.ehpa.org/about-heat-pumps/ (accessed Mar. 20, 2023).

[12] K. T. högskolan, K. I. E. and M. e R. I. of T. K. Eric Granryd, *Refrigerating engineering*.

[13] “kigali amendment - Cerca con Google.” https://www.google.com/search?q=kigali+amendment&oq=&aqs=chrome.0.35i39i362l7j69i59i450.170090j0j7&sourceid=chrome&ie=UTF-8 (accessed Mar. 20, 2023).

[14] “ANSI/ASHRAE Addendum g to ANSI/ASHRAE Standard 34-2016,” 2018, Accessed: Mar. 20, 2023. [Online]. Available: www.ashrae.org

[15] S. V. Shaik and T. P. A. Babu, “Thermodynamic performance analysis and flammability study of various new ozone friendly non azeotropic refrigerant mixtures as alternatives to replace R22 used in residential air conditioners,”

International Journal of Heat and Technology, vol. 36, no. 4, pp. 1470–1481, Dec. 2018, doi: 10.18280/IJHT.360441.

[16] B. T. Austin and K. Sumathy, “Transcritical carbon dioxide heat pump systems: A review,” *Renewable and Sustainable Energy Reviews*, vol. 15, no. 8, pp. 4013–4029, Oct. 2011, doi: 10.1016/J.RSER.2011.07.021.

[17] X. Liu, Y. Hu, Q. Wang, L. Yao, and M. Li, “Energetic, environmental and economic comparative analyses of modified transcritical CO2 heat pump system to replace R134a system for home heating,” *Energy*, vol. 229, p. 120544, Aug. 2021, doi: 10.1016/J.ENERGY.2021.120544.

[18] “Heat Pumps – Analysis - IEA.” https://www.iea.org/reports/heat-pumps (accessed Mar. 20, 2023).

[19] Chen, J., Dai, Y., & Wang, R. (2015). “Comparison Study on Domestic Photovoltaic/thermal, Photovoltaic and Solar Thermal Systems Based on Validated TRNSYS Model.”

[20] Sporn P, Ambrose ER. (1995) The heat pump and solar energy, in World symposium onapplied solar energy. Phoenix, Arizona, USA.

[21] M. Zhu, H. Xie, B. Zhang, and X. Guan, “The Characteristics of the Evaporator/Evaporator for Direct Expansion Solar Assisted Heat Pump System,” *Journal of Power and Energy Engineering*, vol. 01, no. 05, pp. 73–76, 2013, doi: 10.4236/jpee.2013.15012.

[22] E. Bisengimana, J. Zhou, M. Binama, G. Nyiranzeyimana, and Y. Yuan, “Numerical investigation of PVT coverage on an integrated building-solar-heat pump system: Technical and economic study,” *Solar Energy*, vol. 249, pp. 507–520, Jan. 2023, doi: 10.1016/j.solener.2022.12.005.

[23] G. Emmi, S. Bordignon, A. Zarrella, and M. De Carli, “A dynamic analysis of a SAGSHP system coupled to solar thermal collectors and photovoltaic-thermal panels under different climate conditions,” *Energy Convers Manag*, vol. 213, Jun. 2020, doi: 10.1016/j.enconman.2020.112851.

[24] F. Busato, R. M. Lazzarin, and M. Noro, “Multisource heat pump system from design to operation: The case study of a new school building,” *International Journal of Low-Carbon Technologies*, vol. 8, no. 3, pp. 88–94, 2013, doi: 10.1093/ijlct/ctt002.

[25] S. Cesari *et al.*, “A Heat Pump-Based Multi-source Renewable Energy System for the Building Air Conditioning: The IDEAS Project Experience,” *Tecnica Italiana-Italian Journal of Engineering Science*, vol. 65, no. 1, pp. 12–22, Mar. 2021, doi: 10.18280/ti-ijes.650102.

[26] N. Sommerfeldt and H. Madani, “In-depth techno-economic analysis of PV/Thermal plus ground source heat pump systems for multi-family houses in a heating dominated climate,” *Solar Energy*, vol. 190, pp. 44–62, Sep. 2019, doi: 10.1016/j.solener.2019.07.080.

[27] Y. Wang *et al.*, “Modeling and operation optimization of an integrated ground source heat pump and solar PVT system based on heat current method,” *Solar Energy*, vol. 218, pp. 492–502, Apr. 2021, doi: 10.1016/j.solener.2021.03.003.

[28] R. Chargui, H. Sammouda, and A. Farhat, “Geothermal heat pump in heating mode: Modeling and simulation on TRNSYS,” *International Journal of Refrigeration*, vol. 35, no. 7, pp. 1824–1832, Nov. 2012, doi: 10.1016/J.IJREFRIG.2012.06.002.

[29] J. Ma, A. S. Fung, M. Brands, N. Juan, and O. Mohammad Abul Moyeed, “Performance analysis of indirect-expansion solar assisted heat pump using CO2 as refrigerant for space heating in cold climate,” *Solar Energy*, vol. 208, pp. 195–205, Sep. 2020, doi: 10.1016/J.SOLENER.2020.07.001.

[30] E. Zanetti, M. Azzolin, S. Girotto, and D. Del Col, “Performance and control of a CO2 dual source solar assisted heat pump with a photovoltaic-thermal evaporator,” *Appl Therm Eng*, vol. 218, Jan. 2023, doi: 10.1016/j.applthermaleng.2022.119286.

[31] E. Zanetti, M. Azzolin, R. Conte, S. Girotto, and D. Del Col, “Experiments and dynamic modelling of dry expansion and flooded evaporators in a CO2 solar assisted heat pump,” *Appl Therm Eng*, vol. 217, Nov. 2022, doi: 10.1016/j.applthermaleng.2022.118964.

[32] A. Zarrella, G. Emmi, J. Vivian, L. Croci, and G. Besagni, “The validation of a novel lumped parameter model for photovoltaic thermal hybrid solar collectors: a new TRNSYS type,” *Energy Convers Manag*, vol. 188, pp. 414–428, May 2019, doi: 10.1016/j.enconman.2019.03.030.

[33] Alberto Scotton, “Analisi di un sistema multisorgente a pompa di calore con pannelli fotovoltaici ibridi,” 2022.

[34] M. Azzolin *et al.*, “Experimental and numerical analysis of a dual-source heat pump with PVT evaporators for residential heating applications.”

[35] "Bordignon S., Emmi G., Zarrella A., De Carli M., “Energy analysis of different configurations for a reversible ground source heat pump using a new flexible TRNSYS Type”, Applied Thermal Engineering, DOI: 10.1016/j.applthermaleng.2021.117413. ISSN: 13594311"

APPENDIX A

Here the results discussed in paragraph 5.2.1:

	T_evap_sim	T_evap_meas	Absolute error (meas-sim)
	[°C]	[°C]	[°C]
A	3.17	4.41	1.24
B	5.87	7.02	1.16
C	-1.09	-0.83	0.26
D	3.84	4.22	0.37
E	3.17	4.95	1.78
F	-3.51	-2.55	0.96
G	-1.69	-0.38	1.31
H	-1.38	-0.76	0.62
I	-5.61	-6.12	-0.51
J	-1.86	-2.67	-0.81
K	-7.44	-7.41	0.03
L	-5.77	-7.25	-1.48
M	-2.30	2.37	4.67
N	-5.17	-7.29	-2.12

Table A1 evaporation temperature

	p_evap_sim	p_evap_meas	Absolute error (meas-sim)
	[bar]	[bar]	[bar]
A	37.87	38.94	1.07
B	40.59	41.64	1.06
C	33.86	33.91	0.05
D	38.54	38.73	0.20
E	37.87	39.56	1.69
F	31.72	32.47	0.74
G	33.32	34.36	1.04
H	33.60	34.11	0.51
I	29.95	29.59	-0.36
J	33.17	32.53	-0.64
K	28.47	28.49	0.02
L	29.82	28.67	-1.15
M	32.78	37.27	4.49
N	30.32	28.85	-1.47

Table A2 evaporation pressure

	Q_evap_sim	**Q_evap_meas**	**Relative error ξ (meas - sim)**
	[Kw]	**[Kw]**	**%**
A	1.62	1.65	2%
B	1.79	1.81	1%
C	1.38	1.40	1%
D	1.66	1.64	-1%
E	2.07	2.17	4%
F	1.63	1.58	-4%
G	1.74	1.77	2%
H	1.77	1.75	-1%
I	2.39	2.17	-10%
J	2.73	2.61	-5%
K	2.22	2.15	-3%
L	2.37	2.16	-10%
M	2.69	2.21	-22%
N	3.32	3.02	-10%

Table A3 heat of vaporization

	Q_GC_sim	**Q_GC_meas**	**Relative error ξ (meas - sim)**
	[Kw]	**[Kw]**	**%**
A	1.98	2.00	1%
B	2.15	2.16	0%
C	1.72	1.73	1%
D	2.02	1.98	-2%
E	2.55	2.62	3%
F	2.08	2.01	-4%
G	2.21	2.22	1%
H	2.23	2.18	-2%
I	3.17	2.90	-10%
J	3.53	3.40	-4%
K	2.99	2.87	-4%
L	3.21	2.95	-9%
M	3.44	3.03	-14%
N	4.44	4.17	-6%

Table A4 heat exchanged at the gas cooler

	P_comp_sim	P_Comp_meas	Relative error ξ (meas - sim)
	[Kw]	[Kw]	%
A	0.54	0.49	-9%
B	0.52	0.49	-7%
C	0.56	0.52	-7%
D	0.53	0.50	-6%
E	0.68	0.62	-8%
F	0.70	0.65	-7%
G	0.69	0.64	-8%
H	0.69	0.63	-9%
I	1.06	1.01	-5%
J	1.06	1.03	-4%
K	1.06	1.02	-5%
L	1.18	1.12	-6%
M	1.19	1.11	-7%
N	1.50	1.46	-3%

Table A5 Compressor's power consumption

	Pot_el_sim	Pot_el_meas	Relative error ξ (meas - sim)
	[Kw]	[Kw]	%%
A	0.72	0.74	3%
B	0.74	0.69	-7%
C	0.64	0.65	2%
D	0.63	0.63	0%
E	0.77	0.78	1%
F	0.64	0.65	1%
G	0.76	0.76	1%
H	0.69	0.71	3%
I	0.70	0.73	4%
J	0.80	0.80	0%
K	0.70	0.72	3%
L	0.59	0.64	7%
M	0.73	0.76	4%
N	0.82	0.84	2%

Table A6 PVT's electrical power production